Global and Planetary Change 191 (2020) 103211

Contents lists available at ScienceDirect

Global and Planetary Change

journal homepage: www.elsevier.com/locate/gloplacha

Research article

Middlesex/*punctata* Event in the Rhenish Basin (Padberg section, Sauerland, Germany) – Geochemical clues to the early-middle Frasnian perturbation of global carbon cycle

Agnieszka Pisarzowska[a,*], R. Thomas Becker[b], Z. Sarah Aboussalam[b], Marek Szczerba[c], Katarzyna Sobień[d], Barbara Kremer[e], Krzysztof Owocki[e], Grzegorz Racki[a]

[a] Institute of Earth Sciences, University of Silesia in Katowice, Będzińska 60, 41-200 Sosnowiec, Poland
[b] Institut für Geologie und Paläontologie, Westfälische Wilhelms-Universität, Corrensstrasse 24, 48149 Münster, Germany
[c] Institute of Geological Sciences, Polish Academy of Sciences, Kraków Research Centre, Senacka 1, 31-002 Kraków, Poland
[d] Polish Geological Institute - National Research Institute, Rakowiecka 4, 00-975 Warszawa, Poland
[e] Institute of Paleobiology, Polish Academy of Sciences, Twarda 51/55, 00-818 Warszawa, Poland

ARTICLE INFO

Keywords:
Early–middle Frasnian
Rhenish Massif
Padberg Formation
Carbon isotope stratigraphy
Middlesex/*punctata* Event
Trace metal geochemistry

ABSTRACT

A positive carbon stable isotope excursion of about 3‰ is documented in the topmost lower Frasnian at Padberg, eastern Rhenish Massif, as a muted record of the worldwide early – middle Frasnian isotopic perturbation (*punctata* Event; up to 6–8‰ shift in both $\delta^{13}C_{carb}$ and $\delta^{13}C_{org}$ elsewhere), comparable with the Appalachian $\delta^{13}C$ curve. This German isotopic signature occurs in a 12 m thick calciturbidite succession and correlates well with the three-step chemostratigraphic pattern known from the Holy Cross Mountains, Poland. It is especially clear in the $\delta^{13}C_{org}$ shifts, whilst $\delta^{13}C_{carb}$ (and elemental geochemical) proxies are partly biased by post-sedimentary alterations. The New York State, Polish, Nevada and Padberg conodont successions place the onset of the major positive $\delta^{13}C$ excursion slightly beneath the early–middle Frasnian boundary, with *Ancyrodella nodosa* (previously *Ad. gigas* form 1) as the main conodont guide species, and coincident with the Middlesex transgression and spread of cold, nutrient-rich, poorly oxygenated water masses. In the light of geochemical proxies, enhanced primary production and oxygen deficiency occurred evidently in the Rhenish Basin during the *punctata* Event. Moderate Hg enrichments in the early Middlesex/*punctata* Event interval suggest a volcanic signature. However, conclusive data from other regions are required to differentiate between effects of the regionally well-known synsedimenary magmatism and of a possible global volcanic trigger for the biogeochemical perturbation.

1. Introduction

The Devonian Period is characterized by a series of global biotic changes in marine and terrestrial ecosystems of different magnitude (e.g. Walliser, 1996; House, 2002; McGhee, 2013). The last overview by Becker et al. (2016) introduced a distinction between 1st to 4th order global events. The chemostratigraphic record of many Devonian global events (e.g. Taghanic, Frasnian-Famennian, Hangenberg) is marked by comprehensive isotopic evidence of worldwide biogeochemical perturbations (e.g. Buggisch and Joachimski, 2006; Becker et al., 2012).

However, significant geochemical anomalies are not only associated with documented 1st or 2nd order global events (Racki, 2005). In particular, unexpectedly large temporal changes in $\delta^{13}C$ values (above 7‰) were discovered by Yans et al. (2007) in the early–middle Frasnian (E–MF) transition in the Ardennes of Belgium, supported by refined, four-step shift patterns from the Holy Cross Mountains (Pisarzowska and Racki, 2012; see also Racki et al., 2004; Pisarzowska et al., 2006; Baliński et al., 2016). Correlative carbon isotope excursions have also been reported from South China (Ma et al., 2008), the western USA (Morrow et al., 2009), the Appalachian Basin of the eastern USA (Lash, 2019), the Western Canada Sedimentary Basin (Śliwiński et al., 2011), northeast Alberta, Canada (Holmden et al., 2006), southwest Siberia (Izokh et al., 2015), and, likely, from Moravia, Czech Republic (see Geršl and Hladil, 2004) and the Russian Platform (Zhuravlev et al., 2006). However, in terms of background $\delta^{13}C$ levels, particular spike magnitudes, and especially the exact timing of the $\delta^{13}C$ shifts in the conodont zonal scheme, a significant paleogeographic variation among the isotope profiles across the E–MF transition records the multifaceted interplay between various regional and global factors (Śliwiński et al., 2011; Pisarzowska and Racki, 2012).

* Corresponding author.
E-mail address: agnieszka.pisarzowska@us.edu.pl (A. Pisarzowska).

https://doi.org/10.1016/j.gloplacha.2020.103211
Received 10 February 2020; Received in revised form 23 April 2020; Accepted 24 April 2020
Available online 04 May 2020

The extended $\delta^{13}C$ excursion interval coincided with the global Timan, Middlesex and the Lower Rhinestreet events (sensu House and Kirchgasser, 1993; House et al., 2000; House, 2002; Racki et al., 2008; Becker et al., 2016), and all four-step changes in the global carbon cycle were collectively called E–MF perturbation by (Racki et al. 2008; Pisarzowska and Racki, 2012). Following a recent refinement of conodont data (Klapper and Kirchgasser, 2016), the major positive $\delta^{13}C$ shift of as much as 6–7‰, begins near the end of the early Frasnian *Palmatolepis transitans* or MN 4 Zone (Lash, 2019), at the level of the sedimentologically defined Middlesex Event. Similarly to Lash (2019), we retain the commonly used term of Yans et al. (2007), the *punctata* Event, for the most characteristic, extended plateau in $\delta^{13}C$ values, which is still largely in the middle Frasnian *Palmatolepis punctata* Zone.

In continental Europe, well-dated and continuous Frasnian successions of Germany could fill a paleoregional gap in the well-proven geochemical signatures of the E–MF isotopic perturbation in the Holy Cross Mountains and Ardennes. Based on precise results of conodont biostratigraphy, this contribution focuses on high-resolution information on $\delta^{13}C$ time series (the organic and inorganic reservoirs), combined with elemental geochemical signatures, across the early-middle Frasnian transition in a Rhenish reference section at Padberg near Adorf (eastern Sauerland, Fig. 1). The $\delta^{13}C$ record reveals some unique characteristics, biased in part by diagenetic processes. Nevertheless, the integrated isotope and elemental signatures conclusively provide an insight into the complex causes of the prolonged biogeochemical perturbation, in the context of both regional and supra-regional controls, such as tectonic and volcanic activities, sea-level variation, and climate evolution. Furthermore, recent more precise biostratigraphic data allows for a critical review of the conodont datings and carbon isotope chemostratigraphy in all regions with a published record of the early–middle Frasnian isotopic perturbation.

The comprehensive discussion of conodont biostratigraphic questions, paired with microfacies, rock magnetic and mineralogic information on the Padberg succession, significantly affected by post-sedimendary alterations such as hematitisation/limonitisation processes, will be presented by the authors in a related contribution.

2. Regional setting and facies aspects

The studied succession is exposed in an abandoned quarry in the northeastern Rhenish Massif (eastern Sauerland) on the eastern slope of the Padberg, ca. 500 m SE of the small village with the same name, and ca. 1.75 km S of Bredelar. The coordinates on the topographic and geological sheets Madfeld, 1:25000 (GK 4518 Madfeld) are x = ^{34} 84,500, y = ^{56} 96,250 (50°23′52″ N, 08°46′17″ E; Fig. 1).

In Middle-Late Devonian times, the area was part of the extensive outer shelf of southern Laurussia (Eder et al., 1977). In terms of the regionally complex tectonics, the near vertical to slightly overturned (at the southern quarry wall) beds belong to the northeastern margin of the first order Ostsauerland Anticline and to the second order Padberg Anticline. In its core lie Givetian volcanic rocks, the so-called Hauptgrünstein (diabase). Intrusive basaltic lavas and volcaniclastics were mined in the near-by Selecta Quarry at the southern flank of the Padberg. They belong to a submarine eruption centre and seamount, the Padberg volcano (Sunkel, 1990). The directly overlying sediments consist of Givetian-Frasnian dark-grey, fossil-rich turbiditic limestones, the Padberg Limestone (Paeckelmann and Kühne, 1936), and intercalated, dark-grey, poorly fossiliferous shale (Flinz shale). Both are characteristic for the Padberg Formation (Ribbert et al., 2006), with the Padberg Quarry as its type section. The Brilon Reef grew contemporaneously with the volcanic activity to the North and its debris formed the Padberg Formation (Stritzke, 1989, 1990). The nearest outcrop of the reef margin occurs ca. 5 km to the NW. The calciturbiditic sequence is locally followed by pelagic, micritic cephalopod limestone with abundant goniatites (Burgberg Formation). This reflects the expansion of condensed pelagic seamount facies in the higher part of the middle Frasnian (Stritzke, 1989).

3. Lithologic succession and facies

The Padberg Quarry exposes from north to south ca. 250 m individual beds with a total thickness of ca. 32 m. During fieldwork in 2014 and 2016, only the upper, ca. 12 m thick succession was sampled, and subdivided into 144 layers (Fig. 2). Three lithologic sets are distinguished, with a silty shale-enriched middle portion (set B), separating two turbiditic limestone-dominated units (sets A and C):

A - Dark-grey, thin- to medium bedded, bioclastic limestones, separated irregularly by fossil-poor, platy to thickly fissile, shaly intervals up to 0.6 m thick (mudstones in. petrological terms, because dominated by quartz and 2 M1 muscovite).

B - Two non-fossiliferous, dark grey to black, silty shale units, maximally 0.5 m thick, separated by micritic and marly limestones (total thickness 1.1 m; beds 119–125). A uniquely, slightly ash-looking horizon, 2 cm thick, occurs in the uppermost part (bed 124ash).

C - Typically medium- to -thick-bedded, grey, bioclastic limestones (total thickness 3.2 m; beds 126–144), with subordinate shaly intercalations.

Although there are no significant successional changes of mineralogy in the profile, some stratigraphic trends are visible: (i) increase of hematite content relatively to goethite in the upper part of the section (set B and C; this yellowish and reddish interval was marked as the altered zone); (ii) small increase of kaolinite content in the upper part (set B and C); (iii) transition from more illite-smectite in the lower part to more muscovite in the upper one.

The Padberg succession includes a typical Frasnian fore-reef talus, which is possibly associated with a calcareous ooze input from back-reef areas, induced by episodic heavy storm action, as inferred from ecologically mixed bioclastic accumulations. It was originated from the southern margin of the Brilon Reef, where extensive subtidal crinoid-algal forests must have grown. On the other hand, laminated lithofacies of set B are interpreted as a depositional record of pelagic rain pulses from blooming plankton in the near-surface zone.

4. Samples and methods

The main subject of the multidisciplinary analyses were 126 samples taken during fieldwork in 2014 and 2016 by the Polish group. The numbering of samples (marked by Pd) corresponds to the successive numbers of layers. The conodont stratigraphy is based on 14 samples taken independently by R.T. Becker (marked by P).

The mineralogy of 31 samples was determined by XRD analysis of randomly oriented powder specimens using a Thermo ARL X'tra diffractometer at the Institute of Geological Sciences PAS in Kraków, Poland. XRD analyses of clay-mineral (< 2 μm) fractions were performed for samples Pd: 104, 124, and 124top. Thirty-eight samples were powdered and geochemically analysed at the Bureau Veritas Acme Labs Canada Ltd. Major, minor and rare elements were analysed using inductively coupled plasma atomic emission spectrometry (ICP-AES) and inductively coupled plasma mass spectrometry (ICP-MS) methods. The reliability of the analytical results was examined based on the analyses of several international standard reference materials and on duplicate measures of several samples. The precision and accuracy of the results were better than ± 0.05% (mostly ± 0.01%) for the major elements and commonly better than ± 1 ppm for the trace elements.

The isotope compositions of carbonate were determined for 44 samples. Powdered bulk-rock samples were analysed for $\delta^{13}C$ and $\delta^{18}O$ using a Kiel IV Carbonate Device connected to a Finnigan Delta Plus isotope ratio mass spectrometer in a Dual Inlet system at the Institute of Geological Sciences PAS in Warsaw, Poland. Samples reacted with purified H_3PO_4 at 70 °C. A calibration to international standards (NBS 18, NBS 19 and IAEA-CO-9) was made per every ten samples. Isotope ratios are reported as $\delta^{13}C_{carb}$ and $\delta^{18}O$ values and expressed relative to

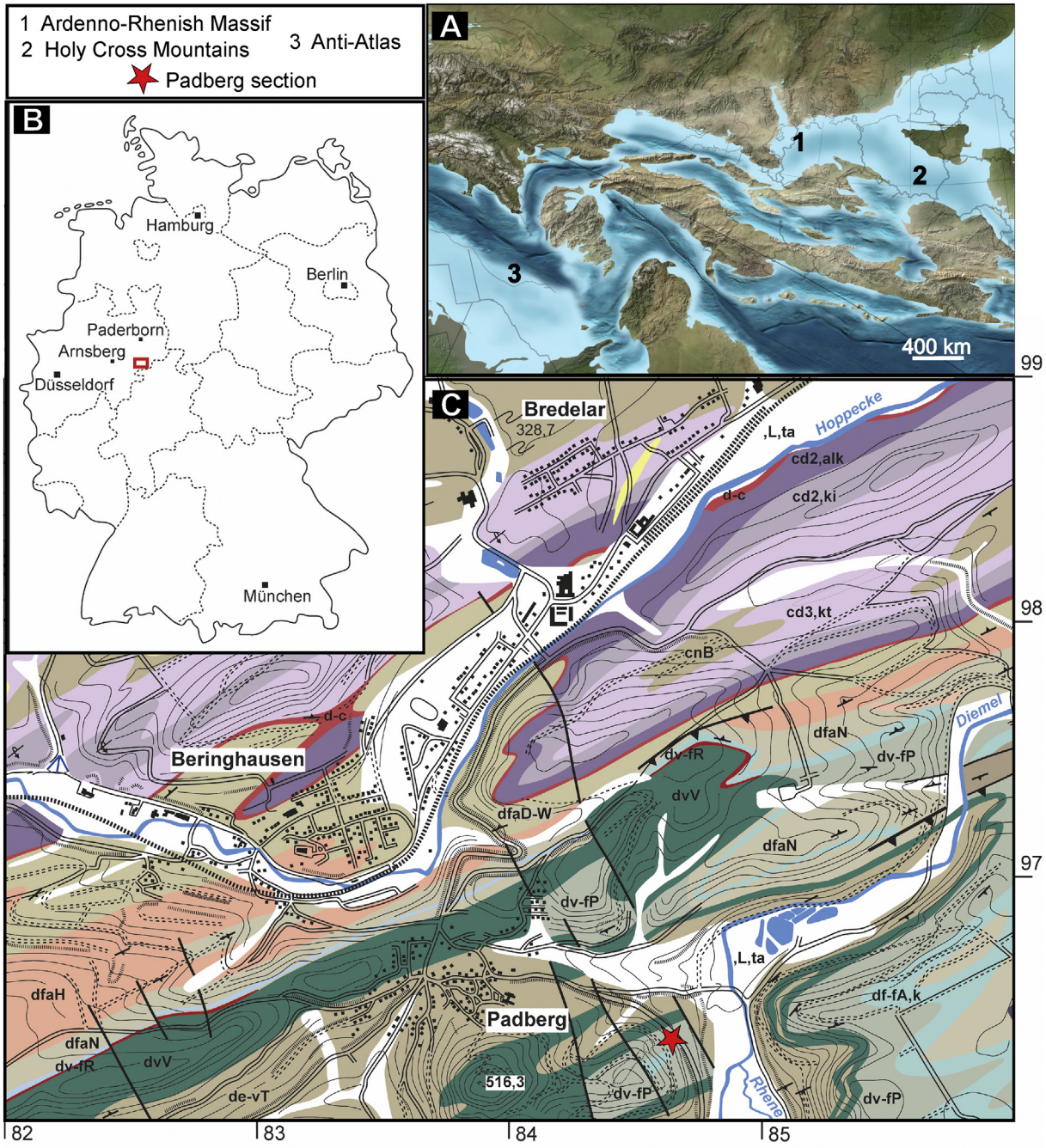

Fig. 1. Location of the Rhenish Massif in (A) the late Devonian Laurussia–peri-Gondwana contact (after Blakey, 2011) and Padberg Quarry in (B–C) Germany on geological sheet 4518 Madfeld (northeastern Sauerland, Ribbert et al., 2006, updated). Abbreviations: de-vT = early/middle Givetian "Tentaculite Beds", dvV = "Hauptgrünstein" (middle Givetian metabasalts and pyroclastics), dv-fR = hematitic iron ore, dv-fP = Padberg Formation (middle Givetian to early middle Frasnian), df-fA, k = Burgberg Formation ("Adorf Limestone", middle Frasnian to early Famennian), dfaN = "Nehden Beds" outside the Brilon Reef (early Famennian), dfaH = Hemberg Formation (middle/early upper Famennian), dfaD-W = "Dasberg and Wocklum Beds" in basinal facies (late/latest Famennian), d–c = Hangenberg Formation (topmost Famennian – early Tournaisian), cd2, alk = Kahlenberg and Hardt Formations (Lower Alum Shale and "Kieselschiefer", middle Tournaisian to early Viséan), cd2, ki = Hillershausen Formation ("Kieselkalk", ca. middle Viséan), cd3, kt = Bromberg Formation ("kieselige Übergangsschichten", late Viséan), cnB = Bredelar Formation (late Viséan to Serpukhovian), L, ta = Quaternary terraces.

the Vienna Pee Dee Belemnite (V-PDB) standard. The measurement precision (1σ) is better than 0.05‰ for $\delta^{13}C$ and 0.15‰ for $\delta^{18}O$, respectively.

Organic matter for analyses was recovered from micritic partings (wackestones) and shales in 42 samples. Powdered samples reacted with 10% HCl for 8 h at 60 °C in a water bath. Following dissolution, the residues were repeatedly rinsed with deionized water. Mineralogical analyses of the acidized residue revealed trace amounts of carbonate in a few samples. For these samples, the procedure was repeated three times using a Sonic Ultrasonic Processor to disintegrate aggregates in which carbonate grains are probably coated by clay-minerals or organic matter. This procedure was ineffective for ten samples (Supplementary Data 1, SD 1).

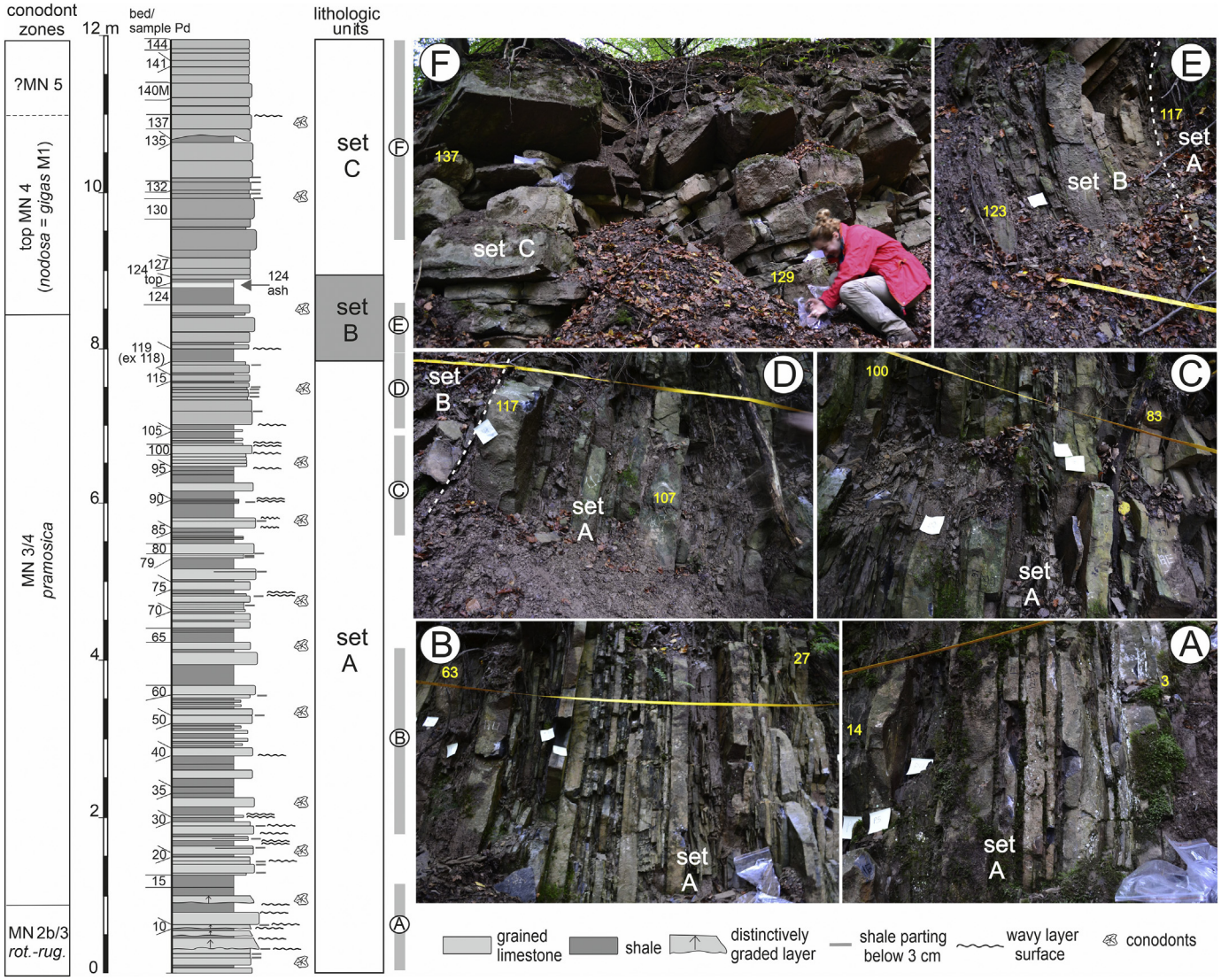

Fig. 2. Lithologic succession of the Frasnian carbonate strata at Padberg Quarry and field photos of different lithologies (taken by K. Owocki). Note thin to medium bedding of calciturbidites, alternating with platy-fissile mudstone (shales) partings in set A (photos A–D), contrasting with more shaly (photo E) and thicker limestone layering (photo F) of overlying sets (B and C, respectively).

5. Conodont dating and correlations

The section is characterized by very abundant conodont assemblages, commonly with several hundred specimens in one normal-sized (2–3 kg) sample. For the early-middle Frasnian we apply the Montagne Noire zonation of Klapper (1989), with updates in Ji and Ziegler (1993), Klapper (1997), Aboussalam and Becker (2007), Bardashev and Bardasheva (2012), and Klapper and Kirchgasser (2016). In order to prevent any misunderstandings, we prefer to name all biozones after their index species but give the MN numbering in addition (Fig. 3). However, early-middle Frasnian zonations are further complicated by biofacies influences, which may result in the episodic or local absence or strongly fluctuating abundances of index taxa.

The lowest samples provided faunas typical for the *Ancyrodella rotundiloba rotundiloba* (Sub)Zone (upper MN Zone 2, basal Frasnian, Klapper, 1997). Due to the complete absence of *Palmatolepis rugosa*, it is not possible to fix locally the base of the MN Zone 3. Because of the entry of *Ad. pramosica*, we place bed 13 at the base of the *pramosica* Zone, which base is correlated with the upper MN 3 Zone. An important newcomer in the same bed 21 is *Ad. alata*, which appears elsewhere in the upper part of the *rugosa* Zone (higher MN Zone 3, Klapper and Kirchgasser, 2016).

Sample P 123 yielded the most important fauna. The distinctive *Ancyrodella nodosa* enters, which has been revised by Klapper and Kirchgasser (2016). This is the same species as *Ad. gigas* form 1 sensu Klapper (1989). It can be strictly separated from the true *Ad. gigas* (= form 3 sensu Klapper, 1989). *Ad. nodosa* commences globally high in the *transitans* Zone (Klapper and Kirchgasser, 2016) and is used here to define the *nodosa* Zone, re-naming the *gigas* Zone of Vandelaer et al. (1989). An important first occurrence of *A. nodosa* lies at the base of the Middlesex Shale in New York State (Over et al., 2003), which marks the hypoxic Middlesex Event sensu House and Kirchgasser (1993). It slightly pre-dates the appearance of *Pa. punctata* in the overlying basal Cashaqua Shale. The entry of *Ad. nodosa* (= *Ad. gigas* M1) approximates the base of *Pa. punctata* and markes the onset of the *punctata* Event in the C-isotope record (Event III of the E–MF isotopic perturbation) of various authors (see Racki and Bultynck, 1993, and Chapter 6.2.1). The term Middlesex Event can be used alternatively.

There are common *Pa. transitans* in sample P 137 but no *Pa. punctata*. This suggests that the basal *punctata* Zone (MN 5 Zone) has not yet been reached in the sampled succession. Graphic correlation (Klapper, 1997; Klapper and Kirchgasser, 2016) of the continuing association of

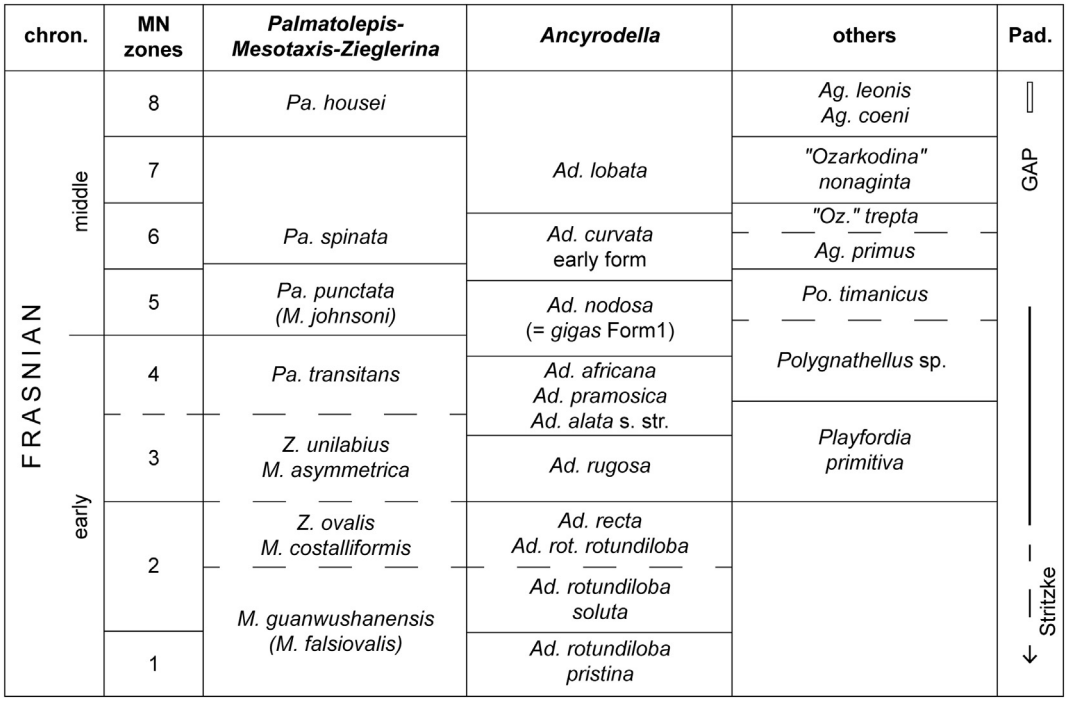

Fig. 3. Lower-middle Frasnian conodont zonations, showing the entry of index species of Ancyrodella, Mesotaxis, Zieglerina, Palmatolepis, and other genera, and of the stratigraphic range of the studied succession at Padberg (right column). Abbreviations: *Ad.* = *Ancyrodella*, *Ag.* = *Ancyrognathus*, *M.* = *Mesotaxis*, *Pa.* = *Palmatolepis*, Pad. – Padberg, *Po.* = *Polygnathus*, *Z.* = *Zieglerina*, chron. – chronostratigraphy.

Ad. nodosa and *Ad. pramosica* in sample P 137 supports this view. However, Pisarzowska et al. (2006) recorded from Śluchowice, sample 37, a direct *pramosica-punctata* co-occurrence at the base of the *punctata* Zone (MN 5 Zone), and therefore the middle Frasnian zone is doubtfully shown in the topmost Padberg succession in Fig. 2.

6. Elemental geochemistry

The Padberg section includes alternating limestones and shales, and this lithological differentiation is evidenced by enrichment/depletion patterns in Supplementary Data 1. For the purpose of more convenient interpretations, we use Al-normalization (element/Al) and enrichment factors ($X_{EF} = X/Al_{sample}/X/Al_{standard}$, Tribovillard et al., 2012; SD 1).

Small differences in the chemical composition between upper and lower parts of the succession are visible. SiO_2, TiO_2, K_2O and Al_2O_3 contents of the carbonate samples have higher values in the lower and middle (samples Pd 1 to Pd 126) and the topmost (Pd 142 to Pd 144) parts of the sections, and lower CaO contents in opposite to most parts of set C (Pd 128 to Pd 141). FeO and MnO have higher values in set B and in the lowest part of set C. Additionally, the MnO content is distinctly lower in the lower part of the section (set A and lowest part of set B; Pd 1 to Pd 119) in comparison to middle and upper parts (sets B and C). The C_{org}/P ratios range from 0.8 to 69.0 with the highest values in set A and lower part of set C, and with the lowest values in set B. The measured Th/U ratios for most carbonate-rich samples of the *pramosica* and bottom and top parts of *nodosa* zones show values > 1. Lower Th/U ratios (< 1), occur in the middle part of set C (from Pd 128 to Pd 140 M). The shale samples from sets A and B reached Th/U ratio < 3, and only shale samples from set B show values > 3. The Th/U ratio shows a good correlation with Mo/Al (Spearman correlation $R = -0.74$). Strong enrichments of Mo, As, Sb and U are observed in the upper part of set C.

The detailed results of trace elements of limestone and shale samples from Padberg are tabulated in the Supplement Data 1.

7. Evolution of sedimentary conditions

7.1. Input of terrigenous material, paleoproductivity and redox conditions

Abrupt changes in mineral and element assemblages of the two distinct types of rocks at Padberg indicate changes in depositional conditions and variable detrital sedimentation in a basin with an episodic influx of proximal to distal calcareous turbidites, particularly during the *pramosica* Zone and the base of the *nodosa* Zone (set B). The increase of Al vs. Ti contents in sets B and C, in conjunction with a highly matured mineralogical composition increased content of kaolinite and hematite(SD 2) in comparison to set A, suggests changes of the weathering regime, from an arid/cooler to a more humid/warmer climate setting (Kiipli et al., 2012) or to the input of more strongly weathered material (e.g. Kołtonik et al., 2018) in the *pramosica/nodosa* zonal boundary interval. Retallack and Huang (2011) calculated atmospheric CO_2 level (based on pedotype paleosols) for this interval. In the opinion of these authors, the deposition of the Middlesex Shale took place at times of a transient greenhouse climatic spike (warm and wet) related to a large increase in atmospheric CO_2.

There is a significant increase in the TOC content and in the TOC/P (C_{org}/P) ratio in set C. This increase precedes elevated Mo, Sb and U concentrations, but is corresponding to low values of Th/U ratio (< 1 for limestone and < 3 for shale), which are traceable for dysoxic bottom-water conditions (Fig. 4). The higher values of the C_{org}/P ratio correspond to higher TOC values (generally above 1%) and are indicative for an increase of productivity (Algeo and Ignall, 2007). Simultaneous increase of C_{org}/P ratio and decrease of Th/U ratio are characteristic for a higher productivity and periodically oxygen restricted conditions. The lowest Th/U ratio during the *nodosa* Zone are correlated with higher concentrations of Mo, Sb and U (Fig. 4). What is unusual in the present case, As enrichments exceed these of Mo, and Sb, which are also relatively high (Fig. 5). Uranium is relatively less enriched than As, Sb and Mo and the maximum U_{EF} values precede the anomalous As_{EF}, Mo_{EF}, and Sb_{EF} values. Such specific trace metal enrichments have been reported from active and ancient mud volcano

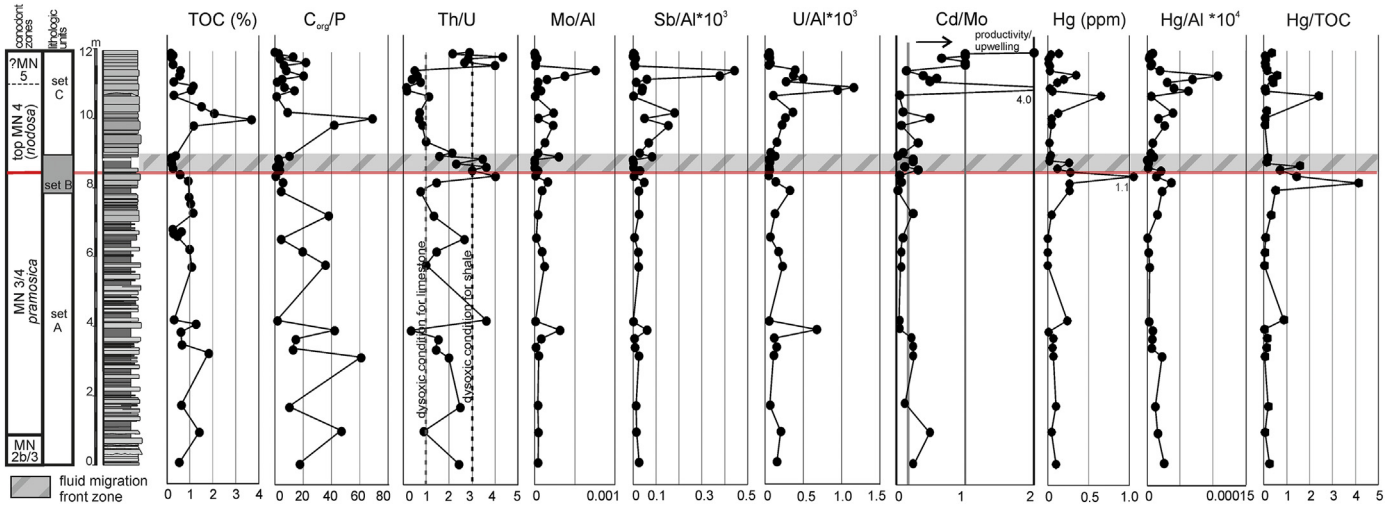

Fig. 4. Composite plot of the Frasnian Padberg section (see Figs. 2 and 6) showing organic carbon and Al-normalized inorganic proxy data. Shaded area represents the fluid migration front zone.

systems (see summary in Tribovillard et al., 2013), because As and Sb abundance in seawater is very low and only a specific mechanism fosters the transfer of these elements from seawater to sediment. Simultaneous significant enrichment in Mo, As and Sb and positive correlation with Fe_2O_3 suggest scavenging them by the Fe-particles and trapping in authigenic minerals (Burdige, 2006).

Cd/Mo ratios are differentiated between hydrographically restricted basins (< 0.1) and upwelling settings (> 0.1; Sweere et al., 2016). Cd/Mo ratios are variable through sets A and B (from 0.05 to 0.50; Fig. 4) and suggest the fluctuation from a slightly more to a less oxygen-deficient basin. In the middle part of set C (Pd 136 and Pd 137), the values significantly increase (4.0) and show high values to the top (~1.0).

7.2. Hydrothermal and volcanic activity

Submarine hydrothermal and volcanic activity is well documented in the Rhenish Massif during the Givetian – early Frasnian (Von Raumer et al., 2017). In the eastern Sauerland, the main episode of basaltic volcanisms occurred in the middle Givetian (e.g. Sunkel, 1990), followed by subordinate volcaniclastic eruptions and hydrothermal exhalations, especially of hematite-rich brines that were siliceous at the exhalation centres and that mixed with micrite laterally. The regional volcanism (volcaniclastic deposition) and hydrothermalism lasted locally into the early and lower part of the middle Frasnian (Bottke, 1965; Sunkel, 1990; Stritzke, 1990; Nesbor et al., 1993; Aboussalam, 2003; Ribbert et al., 2006), but in the case of carbonatic iron ores it is commonly difficult to distinguish the primary hydrothermal influx from common secondary, metasomatic mobilisations of Fe-rich fluids.

As noted above, the thick Padberg volcanites predate and underlie the Padberg Formation. In the eastern Sauerland, close to Padberg, massive siliceous or carbonatic hematite ore bodies that were exploited in extensive mines formed in the Givetian and early Frasnian by submarine hydrothermal exhalation (Lahn-Dill ore type; Nesbor et al., 1993), in times of decreased basaltic volcanism or at the end of volcanic activities (e.g. Bottke, 1965). However, at the famous Martenberg, a few km to the SSE of Padberg, the regionally youngest volcaniclastics

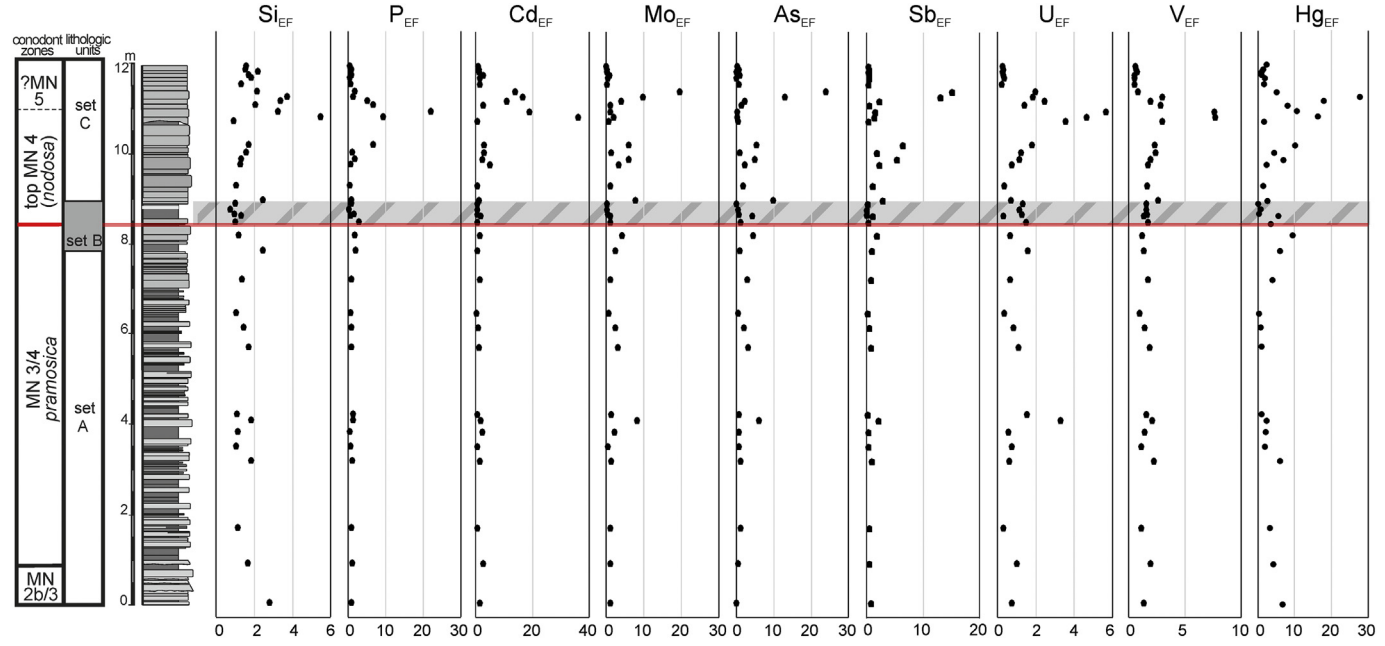

Fig. 5. Enrichment factors of key minor elements at the Frasnian Padberg succession (see Figs. 2 and 6).

and iron ores accumulated around the early–middle Frasnian transition (Ziegler, 1958; Aboussalam, 2003). Episodic influx of fine volcanic ash could have some contribution to a higher illite-smectite content relatively to muscovite in the lower part of the studied profile (SD 2). Mercury concentrations, a worldwide tracer for volcanic (Pyle and Mather, 2003), and submarine hydrothermal paroxysms (Higueras et al., 2013), are higher in most of investigated carbonate samples than in average marine carbonates (Hg > 0.04 ppm; Fig. 4). Two shale samples (Pd 122 and Pd 135) show also a higher Hg content in comparison to the post-Archean Australian shale (Hg > 0.6 ppm). A positive Hg anomaly occurs in set B, while, higher enrichments in Hg is recorded from the middle part of set C (Pd 133 to Pd 140B), with an average Hg_{EF} of 15 (Fig. 5).

Recent studies documented that the Kola alkaline magmatism (Wu et al., 2013) and the first phase of magmatic activity of the Vilyui paleorift (eastern Siberia, Polyansky et al., 2017; Tomshin et al., 2018) were initiated at ca. 380 Ma, i.e. during the *transitans-punctata* time interval (see timescale in Becker et al., 2012). Recently, increased Hg concentration was documented for the late Frasnian Kellwasser Crisis (Racki et al., 2018; Racki, 2020). On the other hand, there is recognized hydrothermalism at the early-middle Frasnian transition of the eastern Sauerland (e.g. Bottke, 1965). The record of the volcanic and especially submarine hydrothermal activity in the studied section is unclear due to secondary (post-diagenetic) processes. Therefore, further research has to search for trace element signals in other regions and to clarify whether the hydrothermal deposits of the eastern Sauerland may carry also synsedimentary Hg enrichments.

8. Carbon isotope chemostratigraphy

8.1. Diagenetic alterations

The existence of small amounts of ankerite/dolomite (SD 2), a mineral commonly considered as secondary mineral (forming cements), can indicate that the succession underwent some degree of diagenesis. Cementation with ankeritic/dolomitic minerals is one of the first steps of diagenesis, and sample Pd 125 contains up to 2% of ankerite/dolomite, indicating similar origin of hematite/goethite in this sample. Hematite (more abundant in the upper part of the section) and goethite (more abundant in the lower part of the section) are the main secondary iron minerals (Fig. 6, SD 2). Variations of the ratio of goethite to hematite up section can be explained by gradual changes of oxidation conditions, or by post-sedimentary oxidation of primary pyrite (Mahoney et al., 2019) in the upper part (sets B and C). The second explanation is more favourable as the hematite-ankerite/dolomite-bearing mineralization (doillite sensu Nieć and Pawlikowski, 2019), occurring in the upper part of set B and most of set C (Fig. 6) likely reflects a local migration of oxidizing, Mn- and ^{18}O-enriched fluids along fractures and faults (e.g. Nieć and Pawlikowski, 2019). Diagenetic fluids in carbonate rocks generally contain comparatively insignificant amounts of secondary carbon; therefore, $\delta^{13}C$ values have a higher preservation potential than oxygen isotopes (Banner and Hanson, 1990). The primary carbon isotopic composition may be altered in case that the stabilization occurs in system open for ^{12}C-enriched CO_2 derived from the remineralisation of organic carbon (Allen and Matthews, 1982; Joachimski, 1994). The input of ^{13}C-depleted CO_2 should shift the carbon isotope composition to lower values. In the studied section, the dolomite/ankerite mineralization is a trace component ($\leq$1%) and, therefore it had no significant effect on the isotope signature (compare Holser, 1997; Buggisch et al., 2003).

Many authors demonstrated that diagenesis under oxygenated conditions can enrich organic matter in ^{13}C (e.g. Sackett and Thompson, 1963; Fruedenthal et al., 2001; Marynowski et al., 2017). The conodont alteration index values (ca. 4) indicate that thermal maturation affected the Padberg section uniformly. Furthermore, the lack of covariance of TOC and $\delta^{13}C_{org}$ in the studied section (R = 0.11) suggests that bottom- and pore-water conditions influenced insignificantly the measured $\delta^{13}C_{org}$ values.

Consequently, the determined $\delta^{13}C_{carb}$ and $\delta^{13}C_{org}$ values in sets A and C reflect largely the approximate primary marine values. Significant changes of the geochemical signature took only place at the silty shale unit (upper part of set B) forming the fluid migration front zone (Fig. 6; samples Pd 123 – Pd 125; compare Buggisch and Joachimski, 2006), where $CaCO_3$ was partialy removed, while organic matter and pyrite were probably oxidized.

The Padberg succession reveals Frasnian background $\delta^{13}C_{carb}$ values (~1‰, see Pisarzowska and Racki, 2012) throughout sets A and B (Fig. 6, SD 1). A negative $\delta^{13}C_{carb}$ shift, corresponding to Event II sensu Pisarzowska et al. (2006), with peak value of −7.9‰ in sample Pd 125, precedes a distinctive positive $\delta^{13}C_{carb}$ excursion. This Event III (sensu Pisarzowska et al., 2006) or the main *punctata* Event (sensu Yans et al., 2007), with values of about 3‰, occurs in the basal set C, above the *pramosica-nodosa* conodont zonal boundary (correlative with the *transitans-punctata* zonal boundary sensu Racki and Bultynck, 1993; Pisarzowska et al., 2006). A gradually decreasing shift to a value of −0.5‰ (Fig. 6), followed by a return to values around 1‰, occur in the upper part of set C.

The $\delta^{13}C_{org}$ record shows a similar pattern as $\delta^{13}C_{carb}$ (Fig. 6). The $\delta^{13}C_{org}$ values obtained across set A (*pramosica* Zone) lie around −27.5‰. In the upper portion of set A, $\delta^{13}C_{org}$ attains values around −25.3‰ in two samples (probably the Inception Event I of Pisarzowska et al., 2006), followed by a shift to −28‰ (?Event II) in set B. The Padberg section reveals a positive $\delta^{13}C_{org}$ excursion (Event III) up to 3‰ at the base of the *nodosa* Zone. In the upper part of the section, $\delta^{13}C_{org}$ values decrease slightly to −26.5‰, which is higher than in the long interval (most of the *pramosica* Zone, set A) before the isotopic perturbation (Fig. 6).

The oxygen isotopes ($\delta^{18}O_{carb}$, Fig. 6) present values in the range − 6.9‰ to −10.3‰ (average − 8.8‰) in set A. The $\delta^{18}O$ values increase up to −3.9‰ (average − 5.1‰) in the upper part of set B and in the basal set C (sample Pd 126). In set C, oxygen isotopes return to values of around −8.7‰.

8.2. Timing of the early–middle Frasnian biogeochemical perturbation in Laurussian sections

The three C-isotopic events (I–III) are part of the long-lasting, four-step early to middle Frasnian E–MF isotopic perturbation (see Yans et al., 2007; Racki et al., 2008), recorded by both the organic and inorganic carbon reservoirs (Pisarzowska et al., 2006; Pisarzowska and Racki, 2012). The revision of the conodont zonal scheme enables a comparison with E–MF $\delta^{13}C$ curves described from other regions, which are known to be variable at intra- and inter-regional scales (Pisarzowska and Racki, 2012; Lash, 2019).

The term *punctata* Event, introduced by Yans et al. (2007), has been widely used for the sequence of isotopic shifts described above, since it was assumed that these occurred within the *Palmatolepis punctata* Zone (MN Zone 5). However, recent biostratigraphic data and increasing precision, especially an improved correlation of parallel ancyrodellid and palmatolepid evolution (Fig. 3), gives a refined time scale for the sequence of E–MF events.

In the Dyminy reef complex succession of the Holy Cross Mountains, Poland, the first appearance datum (FAD) of *Pa. punctata* is only accidentally recorded due to a common delayed entry, partly as late as jointly with the next higher zonal marker *Pa. hassi*. The pelagic guide species is even absent in particular sections (Racki and Bultynck, 1993; Pisarzowska et al., 2006; Vierek and Racki, 2011). The comparison of the conodont sequence with the detailed $\delta^{13}C$ curves (Fig. 6), provide good evidence for differentiated local FADs. The chemo-stratigraphically tuned most reliable FAD for *Pa. punctata* is recognized at Kostomłoty-Mogiłki, where the index species enters in the lower part of the major broad C-isotope excursion ('plateau'), the guide character of

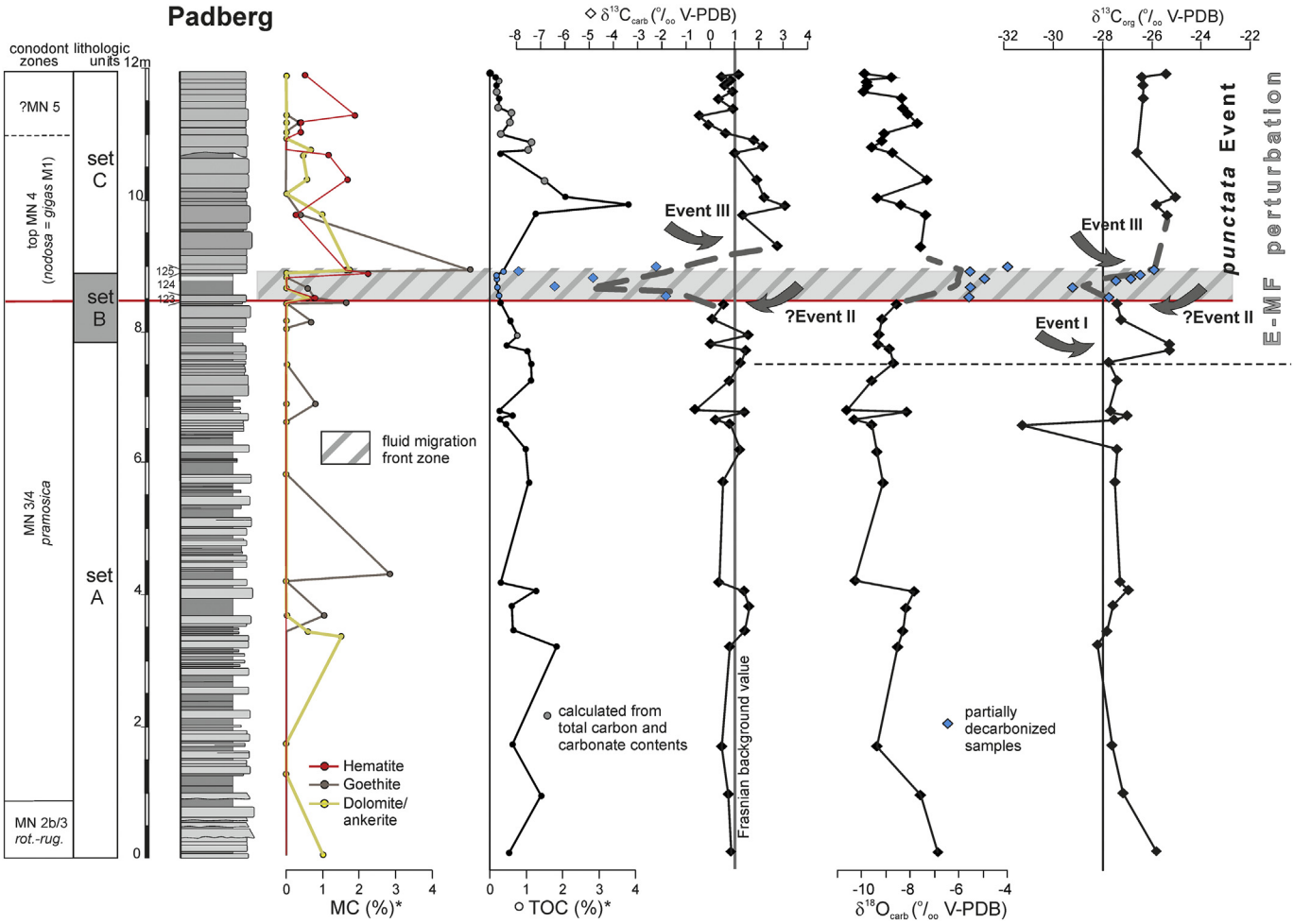

Fig. 6. Lithology, conodont biostratigraphy, mineralogical composition (MC), total organic carbon (TOC), and stable carbon isotope geochemistry for the early-middle Frasnian succession at Padberg (Frasnian background values after Pisarzowska and Racki, 2012), against the regional and global events (see Fig. 7).

E–MF perturbation (=Event III in Pisarzowska et al., 2006, Fig. 10), in relatively deeper-shelf (off-reef) marly facies. In the similar facies of the nearby Radlin area (Baliński et al., 2016), *Pa. punctata* enters after the maximum positive peak of this $\delta^{13}C$ excursion (in sample PR I/6 – fig. 5 therein).

Conversely to dispersal/immigration pattern of palmatolepids during the Middlesex and Rhinestreet sea-level rises (cf. "invasion of pelagic species"; Racki and Bultynck, 1993, Fig. 6), the phylogenetic succession of *Ancyrodella* species across the E–MF boundary is comprehensively documented in Polish sections (Pisarzowska et al., 2006) and elsewhere (see below). The onset of the global *punctata* Event was approximated with the base of the *Pa. punctata* Zone using of the FAD of *Ad. gigas* form 1 as an alternative zonal marker (e.g. Racki and Bultynck, 1993; Morrow et al., 2009; Izokh et al., 2015). In the Appalachian Basin, the base of the middle Frasnian has previously been approximated with the base of the Middlesex Formation and with the Middlesex transgressive-anoxic Event (House and Kirchgasser, 1993; House, 2002). However, Over et al. (2003) showed that *Pa. punctata* enters just above the Middlesex Shale, in the lower Cashaqua Shale, whilst the Middlesex Shale is characterized by the FAD of *Ad. gigas* form 1, which was subsequently synonymized with *Ad. nodosa* (Klapper and Kirchgasser, 2016). As shown in the graphic correlation chart of Klapper (1997), the FAD of *Ad. nodosa* (=*gigas* form 1) is in the top part of the *Pa. transitans* Zone (MN 4 Zone). The major $\delta^{13}C$ excursion (Event III) falls in the level of *Ad. nodosa*, which is well established in several Polish sections (Pisarzowska et al., 2006: entry of *Ad. gigas* form 1). It continues well above the entry of *Pa. punctata* both in Poland and in eastern North America (Lash, 2019, Fig. 4).

The critical ancyrodellid zonal boundary is well recognizable at Padberg, with the base of the re-named *Ad. nodosa* Zone below sample P 123 (middle set B). The abundance of *Pa. transitans* and absence of *Pa. punctata* in sample P 137 (middle set C) indicates that the *transitans-punctata* zonal boundary has not yet been reached at that level. Since *Pa. punctata* is known to display facies-controlled late entries in some sections (e.g. in the Holy Cross Mountains), the base of the *punctata* Zone is questionably assumed for the topmost part of set C (Fig. 2). The crucial Event III starts at least 4 m below, at the *Ad. pramosica – Ad. nodosa* zonal boundary (sample P 123; Figs. 6–7). Therefore, guided by the worldwide chemostratigraphical pattern, only the top early Frasnian part of the muted $\delta^{13}C$ plateau occurs evidently in the Padberg section (Figs. 6–7). Event IV of Pisarzowska et al. (2006) is predicted to lie several meters above, in the covered middle Frasnian interval of the Padberg succession. A corresponding but neglected earlier Rhenish record comes also from the Brilon Reef area, from the upper slope of the small atoll on top of the Grottenberg Volcanoe exposed in the Beringhauser Tunnel section (see review of the section by Hartenfels et al., 2016). Buggisch and Joachimski (2006, p. 69) documented a sharp positive $\delta^{13}C$ spike > 4.5‰ (Fig. 7) (but associated with many diagenetically overprinted $\delta^{13}C$ measurements probably connected with the secondary fluid migration) from the proximal reefal debris at the top of the lower cliff, which they assigned to the "Upper *falsiovalis* Zone" (compare sections and facies analyses in Clausen and Ziegler, 1989; Clausen et al., 1991, and Errenst, 1993). However, Stritzke (1989, loc. 3, Niederhof section = Beringhauser Tunnel) reported the oldest *Ad.*

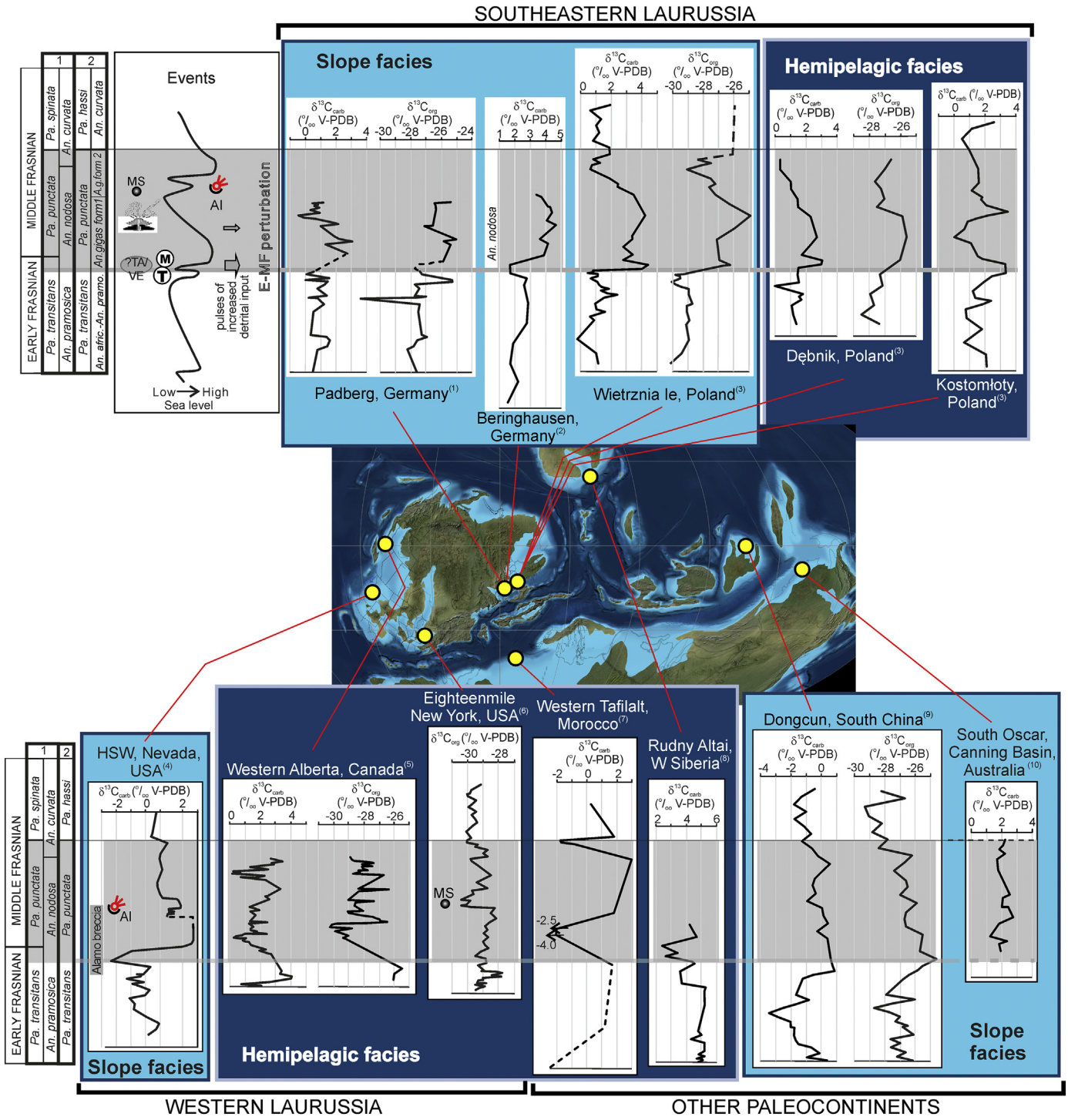

Fig. 7. Records of the early-middle Frasnian *punctata*/Middlesex Event from reef foreslope and hemipelagic settings: (1) present study, (2) Buggisch and Joachimski, 2006, (3) Pisarzowska and Racki (2012), (4) Morrow et al. (2009), (5) Śliwiński et al., 2011, (6) Lash (2019), (7) Becker and Aboussalam (2013), (8) Izokh et al. (2015), (9) Ma et al. (2008), (10) Hillbun (2015), plotted against global biotic and eustatic events. Frasnian paleogeographic reconstruction after Blakey (2016). Sea-level curve compiled after Pisarzowska et al. (2006, fig. 18) and da Silva et al. (2010, fig. 8). Conodont zonation based on the *Ancyrodella* index species (1) revised in these studies and (2) proposed by Racki and Bultynck (1993). Al – position of Alamo impact after Morrow et al. (2009), MS - position of the microtektite-like spherules described by Lash (2019). TA – tectonic activation,VE – volcanic eruption, T – Timan Event, M – Middlesex Event.

gigas (=*nodosa*) from the same interval, which provides a good correlation with the Padberg and Polish isotope Event III.

For the Ardennes, there is no precise correlation of the isotopic curve based on brachiopod shells of Yans et al. (2007) with the conodont ranges in the same general succession. However, the *pramosica* and *nodosa* Zones are regionally well recognizable (Vandelaer et al., 1989).

At the margin of the Miette Carbonate Platform of western Alberta (North America), marked isotopic excursions, both of $\delta^{13}C_{carb}$ and $\delta^{13}C_{org}$, have been found in two sections (AB and K) in the transgressive systems tract (TST) and maximum flooding interval at the base of the lower Perdrix Formation (lower Sequence 5, Śliwiński et al., 2011).

Klapper and Lane (1989) showed that a fauna with *Pa. transitans* and *Ad. gigas* form 1 may occur regionally in the basal Perdrix bed, followed slightly higher by faunas with *Pa. punctata* and *Po. timanicus* (local Zone 2 = MN Zone 5). This suggests a precise correlation of the Perdrix base with the Middlesex Transgression. *Palmatolepis punctata* enters in Section K well above the base of the Perdrix, below a second maximum of $\delta^{13}C_{org}$ and a maximum of $\delta^{13}C_{carb}$ in Section AB.

In the Great Basin of Nevada, the E–MF perturbation was recognized in close association with the Alamo Impact Event (Alamo Breccia Member of the Guilmette Formation, Morrow et al., 2009). *Playfordia primitiva*, which enters at Padberg in the ca. middle part of the *pramosica* Zone, occurs just below the Alamo Breccia Member (Warme and Sandberg, 1995). In this interval, as well as in the first impact-related debris (Unit D), isotopic values are negative. Much more negative values (ca. -3‰), Event II, are recorded from the lower half of their Unit C. Event III, with local $\delta^{13}C_{carb}$ values of only ca. 3‰, but with an amplitude of the isotopic shift of 6‰, begins in the upper part of Unit C, which is characterized by a peculiar, shallow-water pandorinellid biofacies, which cannot be correlated internationally. Since the region is lacking *Pa. punctata*, the *punctata* Zone was instead recognized by the occurrence of *Ad. gigas* (=*nodosa*) in the immediately overlying main impact breccia (Unit B, Warme and Sandberg, 1995), which partly has positive $\delta^{13}C_{carb}$ values. Therefore, the overall succession of marker conodonts and isotopic excursions is well correlated with the Polish and Padberg record (Fig. 7; Morrow et al., 2009; Izokh et al., Fig. 4). The deepening episode recognized by Morrow et al. (2009) at the early *M. johnsoni* level could easily correlate with the transgressive/eustatic Timan Event (House et al., 2000; Becker et al., 2012, 2016). The subsequent Middlesex Event occurred perhaps near the base of the Alamo Breccia Member (T-R cyles in Morrow et al., 2009, Fig. 3; see Fig. 7).

8.3. Timing of the early-middle Frasnian isotopic perturbation in Siberian, Chinese and Gondwanan sections

The E–MF C-isotope pattern is very different in the Rudny Altai Mountains of southern Siberia, a shelf region that faced a different oceanic system. Unusually high $\delta^{13}C_{carb}$ values > 5‰ characterize the *rugosa* Zone (MN Zone 3; Fig. 7), followed by a two-stepped decrease to lower positive values towards the *rugosa/nodosa* Zone boundary (recognizable in Izokh et al., 2015, by the onset of *Ad. gigas*). This interval may partly correlate with Event II, followed by a rapid return to values of up to 5.3‰, the probable major Event III equivalent.

In the Yangsuo Basin of Guangxi Province, South China, two E–MF sections described by Ma et al. (2008) provided detailed carbon isotope curves, which, unfortunately, have no bed-by-bed correlation with the conodont record. At Dongcun, $\delta^{13}C_{carb}$ values are unusually negative through most of the early Frasnian. Event II and the initial sharp positive rise of Event III slightly predate the entry of *Pa. punctata*. *Ancyrodella gigas/nodosa* is locally delayed. At Longmen, records of *Pa. transitans* and *Pa. punctata* are separated by a gap in the section and of the conodont record. There is no correlation with the earlier published conodont succession of Wang (1994). Event II and the locally rather gradual rise towards $\delta^{13}C_{carb}$ values > 2‰ predate the first *Pa. punctata*, as everywhere.

Preliminary data from the northern margin of stable cratonic Gondwana (southeastern Morocco, Becker and Aboussalam, 2013; Fig. 7) yielded constantly lower $\delta^{13}C_{carb}$ values (< 2‰) in a very organic-rich styliolinite facies corresponding to the Timan/Middlesex Event Intervals (*pramosica* to lower *punctata* Zones). Carbon isotope data from Western Australia (Caning Basin, Hillbun, 2015) documented positive $\delta^{13}C_{carb}$ excursion with an amplitude of 2‰ in the middle Frasnian (within MN Zones 5–10; Fig. 7). The excursion was interpreted by the author as the *punctata* Event and related to a major sea-level rise (the Waggon Pass event) at the 5–6 MN zones boundary.

8.4. High-resolution chemostratigraphic pattern

As reviewed above, a strict similarity of our Padberg results with the chemostratigraphic pattern of the Holy Cross Mountains, especially in the $\delta^{13}C_{org}$ time series, is noteworthy. The minor positive $\delta^{13}C$ excursion near the top of the *pramosica* Zone (upper part of MN Zone 4, Event I of the E–MF perturbation) is hardly perceptible in the studied section and saved only in $\delta^{13}C_{org}$ (Fig. 6). The amplitude of the negative $\delta^{13}C$ anomaly recorded at Padberg is the highest among the previously observed (Event II) in Poland (Holy Cross Mountains, Pisarzowska and Racki, 2012), western USA (Nevada; Morrow et al., 2009), China (Dongcun; Ma et al., 2008), and Siberia (Izokh et al., 2015). Lash (2019) suggests that the sharp negative excursion terminating the Middlesex/*punctata* Event of western New York might have been connected with the Alamo (or other still unrecognized) impact-induced destabilization of sea-floor methane hydrates. Recent studies, e.g. on the negative carbon isotopic excursions associated with mass excursions show that massive volcanism (Gutjahr et al., 2017) and thermogenic gas release (Schobben et al., 2019) have a far greater potential to release large amounts of isotopically light carbon into the atmosphere and hydrosphere. On the other hand, however, the negative excursion in the German section uniquely corresponds in fact to the fluid migration front zone (characterized by a clay- and Fe-enrichment and de-carbonated samples; Fig. 6), where diagenetic fluids probably significantly changed the isotopic signature.

The global major $\delta^{13}C$ positive excursion (Event III) of the E–MF isotopic perturbation known worldwide (see above) is well manifested in the Padberg section (Figs. 6–7). The isotope signal (about 3‰) at Padberg is relatively muted, when compared with the 6–8‰ shift in the Holy Cross Mountains and Ardennes, but it is comparable with the Appalachian signature (Fig. 7). Correlations of facies and isotopic records from Eastern Laurussia reef foreslope sections show striking similarities (Pisarzowska et al., 2006; Pisarzowska and Racki, 2012; Fig. 7). The Frasnian Padberg Limestone was deposited on the lower slope of a volcanic seamount south of the steep marginal slope of the Brilon Reef. In relation to the reef margin, the Padberg facies pattern is more distal than the reefal slope setting documented for the middle Wietrznia Beds in the Holy Cross Mountains (Szulczewski, 1971; Vierek, 2007; Vierek and Racki, 2011; see also Baliński et al., 2016). The two $\delta^{13}C$ curves derived from the foreslope succession in the Rhenish Massif show the same chemostratigraphical pattern as on the reef foreslope of Laurussian and Chinese settings (see Fig. 7) The similarity between the $\delta^{13}C$ records confirms an isotopic uniformity of the dissolved inorganic carbon (DIC) of water masses within the distant carbonate shelves.

9. Implications for regional vs. global biogeochemical perturbation

The $\delta^{13}C$ positive excursion of about 3‰ near the early–middle Frasnian boundary is documented for the first time in detail for a German section. It provides not only an additional confirmation for the global nature of the E–MF perturbation in carbon cycling, but also has regional implications thanks to our multidisciplinary approach.

In the context of transgressive–regressive cyclicity, the Timan (base of depophase IIb4 in Becker et al., 2012) and Middlesex (base of depophase IIc) sea-level rises (compare Johnson et al., 1985; House, 2002; Pisarzowska and Racki, 2012) are poorly identifiable in the Padberg fore-reef/turbidite succession, in terms of the limestone microfacies and conodont biofacies. Only few data, such as more frequent micritic lithologies and the entry of pelagic palmatolepids, may suggest a deeper-water setting of exposed upper Padberg limestones. An episode of reduced carbonate supply, associated with the Timan transgressive pulse in the Holy Cross Mountains (Pisarzowska et al., 2006), may be presumed for the mudstone-enriched set B but was probably not a relevant factor in the overall paleogeography of the Brilon Reef area (see Stritzke, 1990).

In the crucial interval referred herein to as the terminal early Frasnian (=basal Middle Frasnian in Pisarzowska et al., 2006), encompassing the upper set B and lower set C, there is local evidence for an increased input of terrigenous material. Whilst there was continuing synsedimentary tectonic activity in the eastern Rhenish Massif associated with the final volcanic phase, which also triggered recurrent turbidites, there is no evidence for significant Eovariscan uplift in the region and in the critical time interval that could have led to increased regional erosion and detrital influxes. Such block faulting events occurred only very locally in the Rhenish Massif in the Givetian (e.g. Salamon and Königshof, 2010), Frasnian-Famennian boundary (Becker et al., 2018), and middle Famennian (e.g. Clausen, 1972). The tectonic events are marked by significant synsedimentary reworking and by the shedding of coarse conglomerates, breccias, debris flows, and olistolites over short distances. In terms of block faulting and uplift, the early–middle Frasnian was a calm period in the Rhenish Massif. There were no clastic wedges in the outer shelf facies realm; only the reef complexes and volcanic seamounts acted as sources for shedding carbonates (Krebs, 1979). Therefore, eustasy was rather a dominating factor for the fluctuating basinward transport of siciliclastics, which were derived from the distal Old Red Continent shelf in the north.

The adopted geochemical proxies permit to postulate that during the higher parts of the early Frasnian (MN Zones 3/4, *pramosica* Zone), the eastern Sauerland sea was a relatively restricted epicontinental basin (reefs and numerous volcanic seamounts formed barriers on the outer shelf), with mostly low oxygen conditions on the seafloor. The oxygen-restricted conditions resulted likely from limited renewal of deep-water in the basin but they were interrupted by the episodes of benthic re-oxygenation associated with episodic heavy storm calcareous turbiditic inputs.

The presence of oxygen-restricted conditions occurring around the early–middle Frasnian boundary and during the *punctata* Zone was described from the Laurussia shelf basin deposits of Poland (Marynowski et al., 2008; Pisarzowska et al., 2014), Timan–Pechora region (Bushnev et al., 2016), Western Canada (Śliwiński et al., 2011; Kabanov, 2018), and Western New York State (Sageman et al., 2003; Blood and Lash, 2018). Early Frasnian oxygen deficiency and high productivity, leading to the mass accumulation of dacryoconarids, occurred also widely on the North African craton of Gondwana, for example in southern Morocco (part of the "Lower Kellwasser" unit of Wendt and Belka, 1991; Upper Styliolinite of Aboussalam and Becker, 2007; Becker and Aboussalam, 2013) basin as well as in southern Algeria and Libya (Lüning et al., 2003, 2004; Mahboubi et al., 2019). Development of anoxic and high productivity conditions is closely related to global E–MF transgression (cycle IIc of Johnson et al., 1985; Middlesex Event, Pisarzowska et al., 2006). At Padberg, the relationships cannot be reliably documented because of extensive post-depositional alterations in the key succession level (set B). However, elevated concentrations of micronutrients, such as Cd and P, and concurrent TOC increases correspond to transgressive pulses near the early–middle Frasnian boundary. The sea-level changes are correlated with the accumulation of redox sensitive trace elements and the positive inorganic and organic carbon isotope excursion, well recognizable in set C (Figs. 4–6). The input of deep, cold, nutrient-rich water masses during the sea-level rise would have first stimulated primary productivity in the surface waters and stimulated expanded more oxygen-deficient conditions in the *nodosa* Zone (top *transitans* Zone) and assumed *punctata* Zone, i.e., during the Middlesex/*punctata* Event (compare with model of Pisarzowska and Racki, 2012; Śliwiński et al., 2012; Crasquin and Horne, 2018). Pyritized spheromorphs observed in the Padberg limestones undoubtedly suggests a reducing sedimentary environment with available iron and sulfur. Additionaly, the absence of benthic fauna indicates not particularly favourable conditions for bottom colonization. Interestingly, laminated depositional fabrics, interpreted as a consequence of pelagic rain from plankton blooms from the near-surface zone (Kremer, 2011), are recognized only in the weak initial phase (set B) of the biogeochemical perturbation. Calciturbiditic re-inputs recorded in the uppermost part of the Padberg section, on one hand could have diluted organic mater and on the other ventilated the sea-bottom, and re-oxidized the sediment-water interface and underlying sediments (Caillaud et al., 2020; compare Rakociński et al., 2016; Broda et al., 2019).

Lack or trace amounts of pyrite in the studied section probably results from its oxidation into hematite during migration of diagenetic solutions. Similar processes of hydrothermal oxidation were proposed in the Holy Cross Mountains (Kowala section) in the middle Frasnian limestones and shales (Marynowski et al., 2008). The processes of the secondary fluid migration, taking place after the lithification of the sediments, caused also partial organic matter oxidation and disguised a record of climatic perturbation observed in the Holy Cross Mountains (i.e., cooling trend – Pisarzowska and Racki, 2012; Baliński et al., 2016). On the other hand, CO_2-greenhouse spikes connected with transient external perturbations to the atmosphere are confirmed, among others, by the presence of large cladoxylopsid trees in New York during the Middlesex Event (Retallack and Huang, 2011). According to the authors, the reason for such abrupt climatic changes may have been massive volcanic eruptions and/or meteorite impacts. Thus, the climatic context of Middlesex/*punctata* Even (i.e. cooling in marine settings vs. continental warming) may be seen as uncertain, but, perhaps, explainable by the low resolution of marine oxygen isotope signature in biogenic apatites (see further discussion in Racki, 2020).

Moderate Hg enrichments in set C of Padberg need a confirmation from other regions in order to separate just regional and more widespread (terrestrial and/or submarine) signatures of volcanisms, and its possible general participation in the global perturbation. The same approval awaits a supposed role of extraterrestrial factors (e.g. of the contemporaneous Alamo Impact; see discussion in Yans et al., 2007 and Hladil et al., 2009), recently revived by Lash (2019) because of the finding of microtektite-like spherules (see also Sim et al., 2015). However, the microspherule horizon reported by Lash (2019) and Hladil et al. (2009) comes from the middle part of the *punctata* $\delta^{13}C$ plateau (Fig. 7), which negates the suggested correlation with the base of the Middlesex Event.

10. Conclusions and final remarks

A stable carbon isotope positive excursion of about 3‰ is documented in the basal *nodosa* Zone (topmost *Palmatolepis transitans* Zone, top MN Zone 4) at Padberg, Rhenish Massif, as a muted record of the worldwide early–middle Frasnian isotopic perturbation. Only the lower part of the $\delta^{13}C$ "plateau" occurs in the Padberg section (as shown by the uncertain conodont datings). The German signature is overall correlative with the chemostratigraphic pattern (Events I–III) from the Holy Cross Mountains. The stratigraphic level of Event IV of Pisarzowska et al. (2006), which terminated the longer-lasting positive $\delta^{13}C$ excursion, is certainly not exposed at Padberg.

Based on the conodont data from Padberg, in comparison with data from the Holy Cross Mountains and New York State, the isotopic Event III (*punctata* Event) occurred near the boundary between the *pramosica* and *nodosa* Zones of the ancyrodellid succession, or near the top of the *transitans* Zone (top MN Zone 4). *Palmatolepis punctata* enters slightly later, within the long-lasting positive $\delta^{13}C$ excursion interval. A critical review of the conodont datings and carbon isotope chemostratigraphy in all regions with a published record of the *punctata* Event suggests that the same timing of $\delta^{13}C$ events is also true for all regions of western North America, Siberia, and South China.

In eastern North America, chemostratigraphical Event III is directly correlated with the transgressive and hypoxic Middlesex Event, which defines the base of the global depophase IIc sensu Johnson et al. (1985). Corresponding correlations of Event III and transgression are also evident in western Canada (e.g. Christina Member of Waterways Formation, lower Hay River Formation), in Nevada (transgression at the base

of the Alamo Breccia Member), in the Holy Cross Mountains, and possibly in the Rhenish Massif. The main Alamo Impact breccia contains the Event III episode, starting in Unit C of Warme and Sandberg (1995), and the first, possibly locally delayed (due to a unique "pandorinellid" biofacies interval in Unit C), *Ad. nodosa* in Unit B. Therefore, possible long-term relationships between the isotopic event and the regional impact destruction of a carbonate platform, as a potential source of CO_2 and CO (Kawaragi et al., 2009; Artemieva et al., 2017), have to be re-considered (Fig. 7).

The $\delta^{13}C_{carb}$ pattern and elemental geochemical proxies are partly biased by post-sedimentary alterations in Padberg succession. Neverheless, enrichments in specific elements (e.g. Hg, As, Sb) observed in Padberg section indicate volcanic activity and/or hydrothermal exhalations during the early-middle Frasnian isotopic perturbation. A rather uncertain volcanic signal is surprising in the context of current data on the timing of Devonian large igneous provinces (LIPs, especially from Siberia; see summary in Ernst et al., 2020 and Racki, 2020). A possible volcanic trigger needs a comprehensive verification for all early and middle Frasnian anoxic events, likely corresponding to CO_2/greenhouse spikes (Retallack and Huang, 2011) and/or negative $\delta^{13}C$ shifts (Schobben et al., 2019).

Analogous to other Laurussian shelf settings, intensified sea water exchange between the epeiric sea and the open waters during transgressive pulse coupled with an increase in nutrient supply to the basin probably enhanced primary production and the development of more oxygen-restricted conditions (see discussion in Sim et al., 2015), as evident in the Rhenish Basin during the *punctata*/Middlesex Event.

Declaration of Competing Interest

The authors declare that they have no known competing financial interests or personal relationships that could have appeared to influence the work reported in this paper.

Acknowledgements

Krzysztof Broda, Michał Rakociński and Michał Zatoń are acknowledged for their extensive help in field works in 2014 and 2016. We thank Dorota Bakowska, Zuzanna Ciesielska, Beata Gebus-Czupyt and Magdalena Radzikowska for their laboratory works. At Münster, Davina Mathijssen processed and picked the conodont samples, Traudel Fährenkemper assisted with the drawing of Figs. 1 and 3. The paper was greatly improved following suggestions by David Bond, an anonymous reviewer, and by guest editor Paul Wignall. This study was supported by the National Science Centre in Poland research grant 2013/08/A/ST10/00717 for G. Racki.

Appendix A. Supplementary data

Supplementary data to this article can be found online at https://doi.org/10.1016/j.gloplacha.2020.103211.

References

Aboussalam, Z.S., 2003. Das "Taghanic-Event" im höheren Mittel-Devon von West-Europa und Marokko. In: Münstersche Forschungen zur Geologie und Paläontologie. 97. pp. 1–332.
Aboussalam, Z.S., Becker, R.T., 2007. New upper Givetian to basal Frasnian conodont faunas from the Tafilalt (Anti-Atlas, Southern Morocco). Geol. Q. 51 (4), 345–374.
Algeo, T.J., Ignall, E., 2007. Sedimentary Corg:P ratios, paleocean ventilation, and Phanerozoic atmospheric pO_2. Palaeogeogr. Palaeoclimatol. Palaeoecol. 256, 130–155.
Allen, J.R., Matthews, R.K., 1982. Isotope signatures associated with early meteoric diagenesis. Sedimentology 29, 797–817.
Artemieva, N., Morgan, J., Expedition 364 Science Party, 2017. Quantifying the Release of Climate-Active Gases by Large Meteorite Impacts With a Case Study of Chicxulub. Geophysical Research Letters 44, 10,180–10,188.
Baliński, A., Racki, G., Halamski, A.T., 2016. Brachiopods and stratigraphy of the Upper Devonian (Frasnian) succession of the Radlin Syncline (Holy Cross Mountains, Poland). Acta Geol. Pol. 66 (2), 107–156.
Banner, J.L., Hanson, G.N., 1990. Calculation of simultaneous isotopic and trace element variations during water-rock interaction with application to carbonate diagenesis. Geochim. Cosmochim. Acta 54, 3123–3137.
Bardashev, I.A., Bardasheva, N.P., 2012. Platform Conodonts From the Givetian-Frasnian Boundary (Middle-Upper Devonian). 90 pp.. Academie of Science, Republic of Tajikistan, Institute of Geology, Seismic Building and Seismology, Dushanbe (Donish Publishing House).
Becker, R.T., Aboussalam, Z.S., 2013. Middle Givetian – middle Frasnian event stratigraphy at Mdoura-East (western Tafilalt). In: Becker, R.T., El Hassani, A., Tahiri, A. (Eds.), International Field Symposium, The Devonian and Lower Carboniferous of northern Gondwana, Field Guidebook. 27. Document de l'Institut Scientifique, Rabat, pp. 143–150.
Becker, R.T., Gradstein, F.-M., Hammer, O., 2012. The Devonian period. In: Gradstein, F.M., Ogg, J.G., Schmitz, M., Ogg, G. (Eds.), The Geologic Time Scale 2012. Elsevier, Amsterdam, Boston, pp. 559–601.
Becker, R.T., Königshof, P., Brett, C.E., 2016. Devonian climate, sea level and evolutionary events: an introduction. In: Becker, R.T., Königshof, P., Brett, C.E. (Eds.), Devonian Climate, Sea Level and Evolutionary Events. Geological Society, London, Special Publications 423. pp. 1–10.
Becker, R.T., Aboussalam, Z.S., Hartenfels, S., 2018. The Frasnian-Famennian boundary mass extinction – widespread seismic events, the timing of climatic pulses, "pelagic death zones", and opportunistic survival. In: 5th International Palaeontological Congress, July 9th to 13th, 2018. Abstract Book, France, pp. 107.
Blakey, R., 2011. Devonian - 375 Ma, Paleogeography of Europe. Deep Time Maps™ Paleogeography.
Blakey, R., 2016. Devonian - 380 Ma, Global Paleogeography and Tectonics in Deep Time Series. Deep Time Maps™ Paleogeography.
Blood, R., Lash, G.G., 2018. FT-02 Stratigraphy and Sedimentology of the Upper Devonian Black Shales of Western New York State With Considerations for Unconventional Reservoir Development. Field Trip Guidebook. Eastern Section AAPG 47th Annual Meeting.
Bottke, H., 1965. Die exhalativ-sedimentären devonischen Roteisensteinlagerstätten des Ostsauerlandes. In: Beihefte zum Geologischen Jahrbuch. 63. pp. 1–147 8 pls.
Broda, K., Marynowski, L., Rakociński, M., Zatoń, M., 2019. Coincidence of photic zone euxinia and impoverishment of arthropods in the aftermath of the Frasnian-Famennian biotic crisis. Sci. Rep. 9, 16996.
Buggisch, W., Joachimski, M.M., 2006. Carbon isotope stratigraphy of the Devonian of Central and Southern Europe. Palaeogeogr. Palaeoclimatol. Palaeoecol. 240, 68–88.
Buggisch, W., Keller, M., Lehnert, O., 2003. Carbon isotope record of Late Cambrian to Early Ordovician carbonates of the Argentine Precordillera. Palaeogeogr. Palaeoclimatol. Palaeoecol. 195, 357–373.
Burdige, D.J., 2006. Geochemistry of Marine Sediments. Princeton Univ. Press, Princeton, N.J.
Bushnev, D.A., Burdelnaya, N.S., Ponomarenko, E.S., Zubova-Kiryukhina, T.A., 2016. Anoxia in the Domanik Basin of the Timan–Pechora Region. Lithol. Miner. Resour. 51 (4), 283–289.
Caillaud, A., Quijada, M., Huet, B., Reynaud, J.-Y., Riboulleau, A., Bout-Roumazeilles, V., Baudin, F., Chappaz, A., Adatte, T., Ferry, J.-N., Tribovillard, N., 2020. Turbidite-induced re-oxygenation episodes of the sediment-water interface in a diverticulum of the Tethys Ocean during the Oceanic Anoxic Event 1a. In: The French Vocontian Basin. Depositional Record In press.
Clausen, C.-D., 1972. Geologie der Cephalopodenkalk-Sattelaufbrüche und ihrer Hüllsedimente in der Attendorn-Elsper Doppelmulde (Sauerland, Rhein. Schiefergebirge). N. Jb. Geol. Paläont. 140 (2), 146–184.
Clausen, C.-D., Ziegler, W., 1989. Die neue Mittel-/Oberdevon-Grenze – ihre Anwendungsmöglichkeiten im Rheinischen Schiefergebirge. In: Fortschritte in der Geologie von Rheinland und Westfalen. 35. pp. 9–30.
Clausen, C.-D., Korn, D., Luppold, F.-W., 1991. Litho- und Biofazies des mittel- oberdevonischen Karbonatprofils am Beringhäuser Tunnel (Messinghäuser Sattel, nördliches Rheinisches Schiefergebirge). In: Geologie und Paläontologie in Westfalen. 18. pp. 7–65.
Crasquin, S., Horne, D.J., 2018. The palaeopsychrosphere in the Devonian. Lethaia 51, 547–563.
da Silva, A.-C., Yans, J., Boulvain, F., 2010. Early-middle Frasnian (early Late Devonian) sedimentology and magnetic susceptibility of the Ardennes area (Belgium): identification of severe and rapid sea-level fluctuations. Geol. Belg. 13, 319–332.
Eder, W., Engel, W., Franke, W., Langenstrassen, F., Walliser, O.H., Witten, W., 1977. Überblick über die paläogeographische Entwicklung des östlichen Rheinischen Schiefergebirges. In: Exkursionsführer Geotagung 77, Exkursion A. 1. pp. 2–11 Göttingen.
Ernst, R.E., Rodygin, S.A., Grinev, O.M., 2020. Age correlation of Large Igneous Provinces with Devonian biotic crises. Glob. Planet. Chang. 185, 103097.
Errenst, C., 1993. Koloniebildende Phillipsastreidae und Hexagonariinae aus dem Givetium des Messinghäuser Sattels und vom Südrand des Briloner Massenkalkes (nordöstliches Sauerland). In: Geologie und Paläontologie in Westfalen. 26. pp. 7–45.
Geršl, M., Hladil, J., 2004. Gamma-ray and magnetic susceptibility correlation across a Frasnian carbonate platform and the search for "punctata" equivalents in stromatoporoid-coral limestone facies of Moravia. Geol. Q. 48 (3), 283–292.
Gutjahr, M., Ridgwell, A., Sexton, P.F., Anagnostou, E., Pearson, P.N., Pälike, H., Norris, R.D., Thomas, E., Foster, G.L., 2017. Very large release of mostly volcanic carbon during the Palaeocene-Eocene Thermal Maximum. Nature 548, 573–577.
Hartenfels, S., Becker, R.T., Aboussalam, Z.S., 2016. Givetian to Famennian stratigraphy, Kellwasser, *Annulata* and other events at Beringhauser Tunnel (Messinghausen Anticline, eastern Rhenish Massif). In: Münstersche Forschungen zur Geologie und Paläontologie. 108. pp. 196–219.

Higueras, P., Oyarzun, R., Lillo, J., Morata, D., 2013. Intraplate mafic magmatism, degasification, and deposition of mercury: the giant Almadén mercury deposit (Spain) revisited. Ore Geol. Rev. 51, 93–102.
Hillbun, C.N., 2015. Re-Evaluating the Late Devonian Mass Extinction: A Geochemical Investigation of the Relationship between Carbon Isotope Fluctuations, Faunal Turnover, and Paleoenvironmental Change Recorded in Upper Devonian Carbonates of the Lennard Shelf, Western Australia. PhD thesis. University of Washington.
Hladil, J., Koptíková, L., Galle, A., Sedláček, V., Pruner, P., Schnabl, P., Langrová, A., Bábek, O., Frána, J., Hladíková, J., Otava, J., Geršl, M., 2009. Early Middle Frasnian platform reef strata in the Moravian Karst interpreted as recording the atmospheric dust changes: the key to understanding perturbations in the punctate conodont zone. Bull. Geosci. 84 (1), 75–106.
Holmden, C., Braun, W.K., Patterson, W.P., Eglington, B.M., Prokopiuk, T.C., Whittaker, S., 2006. Carbon isotope chemostratigraphy of Frasnian sequences in western Canada. In: Summary of Investigations 2006. Saskatchewan Geological Survey, Sask. Industry Resources, Misc. Rep. 2006-4.1, CD-ROM, Paper A-8 1. pp. 1–6.
Holser, T.W., 1997. Geochemical events documented in inorganic carbon isotopes. Palaeogeogr. Palaeoclimatol. Palaeoecol. 132, 173–182.
House, M.R., 2002. Strength, timing, setting and cause of mid-Palaeozoic extinctions. Palaeogeogr. Palaeoclimatol. Palaeoecol. 181, 5–25.
House, M.R., Kirchgasser, W.T., 1993. Devonian goniatite biostratigraphy and timing of facies movements in the Frasnian of eastern North America. In: Hailwood, E.A., Kidd, R.B. (Eds.), High Resolution Stratigraphy. Geological Society Special Publication 70. pp. 267–292.
House, M.R., Menner, V.V., Becker, R.T., Klapper, G., Ovnatanova, N.S., Kuz'min, V., 2000. Reef episodes, anoxia and sea-level changes in the Frasnian of the southern Timan (NE Russian platform). In: Insalaco, E., Skelton, P.W., Palmer, T.J. (Eds.), Carbonate Platform Systems: Components and Interactions. Geological Society, London, Special Publications 178. pp. 147–176.
Izokh, O.P., Izokh, N.G., Saraev, S.V., Dokukina, G.A., 2015. C isotopic variations in the lower–middle Frasnian (lower Upper Devonian) of the Rudny Altai. Geol. Mag. 152, 565–571.
Ji, Q., Ziegler, W., 1993. The Lali section: an excellent reference section for upper Devonian in South China. Courier Forschungsinstitut Senckenberg 157, 1–183.
Joachimski, M.M., 1994. Subaerial exposure and deposition of shallowing upward sequences: evidence from stable isotopes of Purbeckian peritidal carbonates (basal Cretaceous), Swiss and French Jura Mountains. Sedimentology 41, 805–824.
Johnson, J.G., Klapper, G., Sandberg, C.A., 1985. Devonian eustatic fluctuations in Euramerica. Geol. Soc. Am. Bull. 96, 567–587.
Kabanov, P., 2018. Devonian (ca. 388-375 My) Horn River Group of Mackenzie Platform (northwestern Canada) is an open-shelf succession recording oceanic anoxic events. J. Geol. Soc. 176 (1), 29–45.
Kawaragi, K., Sekine, Y., Kadono, T., Sugita, S., Ohno, S., Ishibashi, K., Kurosawa, K., Matsui, T., Ikeda, S., 2009. Direct measurements of chemical composition of shock-induced gases from calcite: an intense global warming after the Chicxulub impact due to the indirect greenhouse effect of carbon monoxide. Earth and Planetary Science Letters 282, 56–64.
Kiipli, E., Kiipli, T., Kallaste, T., Siir, S., 2012. Al_2O_3/TiO_2 ratio of the clay fraction of Late Ordovician–Silurian carbonate rocks as an indicator of paleoclimate of the Fennoscandian Shield. Palaeogeogr. Palaeoclimatol. Palaeoecol. 365-366, 312–320.
Klapper, G., 1989. The Montagne Noire Frasnian (Upper Devonian) conodont succession. In: McMillan, N.J., Embry, A.F., Glass, D.J. (Eds.), Devonian of the World, Proceedings of the Second International Symposium on the Devonian System, Calgary, Canada. 14(III). Canadian Society of Petroleum Geologists, Memoir, pp. 449–468.
Klapper, G., 1997. Graphic Correlation of Frasnian (Upper Devonian) Sequences in Montagne Noire, France, and Western Canada. 321. Geological Society of America, pp. 113–129 Special Paper.
Klapper, G., Kirchgasser, W.T., 2016. Frasnian Late Devonian conodont biostratigraphy in New York: graphic correlation and taxonomy. J. Paleontol. 90 (3), 525–554.
Klapper, G., Lane, H.R., 1989. Frasnian (Upper Devonian) conodont sequence at Luscar Mountain and Mount Haultain, Alberta Rocky Mountains. In: McMillan, N.J., Embry, A.F., Glass, D.J. (Eds.), Devonian of the World, Proceedings of the Second International Symposium on the Devonian System, Calgary, Canada. 14(III). Canadian Society of Petroleum Geology, Memoir, pp. 469–489 (imprint 1988).
Kołtonik, K., Pisarzowska, A., Paszkowski, M., Sláma, J., Becker, R.T., Szczerba, M., Krawczyński, W., Hartenfels, S., Marynowski, L., 2018. Baltic provenance of top-Famennian siliciclastic material of the northern Rhenish Massif, Rhenohercynian zone of the Variscan orogen. Int. J. Earth Sci. 107, 2645–2669.
Krebs, W., 1979. Dervonian basinal facies. Spec. Pap. Palaeontol. 23, 125–139.
Kremer, B., 2011. High productivity of early Silurian sea evidenced by post-bloom macroaggregates. Sediment. Geol. 240, 115–122.
Lash, G.G., 2019. A global biogeochemical perturbation during the Middle Frasnian punctata Event: evidence from muted carbon isotope signature in the Appalachian Basin, New York State (USA). Glob. Planet. Chang. 177, 239–254.
Lüning, S., Adamson, K., Crfaig, J., 2003. Frasnian organic-rich shales in North Africa: Regional distribution and depositional model. In: Arthur, T.J., McGregor, D.S., Caneron, N.R. (Eds.), Petroleum Geology of Africa: New Themes and Developing Technologies. Geological Society, London, Special Publications 207. pp. 165–184.
Lüning, S., Wendt, J., Belka, Z., Kaufmann, B., 2004. Temporal – spatial reconstruction of the early Frasnian (Late Devonian) anoxia in NW Africa; new field data from the Ahnet Basin (Algeria). Sediment. Geol. 163, 237–264.
Ma, X.P., Wang, C.Y., Racka, M., Racki, G., 2008. Isotope and inorganic geochemistry across the Early-Middle Frasnian transition (Late Devonian) on South China carbonate shelf: comparison with the Polish reference. Palaeogeog. Palaeoclimatol. Palaeoecol. 269, 130–151.
Mahboubi, A., Cornée J., J., Feist, R., Camps, P., Girard, C., 2019. Frasnian (Upper Devonian) integrated facies analysis, magnetic susceptibility and sea-level fluctuations in the NW Algerian Sahara. Geol. Mag. 156, 1295–1310.
Mahoney, C., März, C., Buckman, J., Wagner, T., Blanco-Velandia, V.-O., 2019. Pyrite oxidation in shales: Implications for palaeo-redox proxies based on geochemical and SEM-EDX evidence. Sediment. Geol. 389, 186–199.
Marynowski, L., Filipiak, P., Pisarzowska, A., 2008. Organic geochemistry and palynofacies of the Early–Middle Frasnian transition (Late Devonian) of the Holy Cross Mts, southern Poland. Palaeogeogr. Palaeoclimatol. Palaeoecol. 269, 152–165.
Marynowski, L., Pisarzowska, A., Derkowski, A., Rakociński, M., Szaniawski, R., Środoń, J., Cohen, A.S., 2017. Influence of palaeoweathering on trace metal concentrations and environmental proxies in black shales. Palaeogeogr. Palaeoclimatol. Palaeoecol. 472, 177–191.
McGhee, G.R., 2013. When the Invasion of Land Failed: The Legacy of the Devonian Extinctions. Columbia University Press, New York.
Morrow, J.R., Sandberg, C.A., Malkowski, K., Joachimski, M.M., 2009. Carbon isotope chemostratigraphy and precise dating of middle Frasnian (lower Upper Devonian) Alamo Breccia, Nevada, USA. Palaeogeogr. Palaeoclimatol. Palaeoecol. 282, 105–118.
Nesbor, H.D., Buggisch, W., Flick, H., Horn, M., Lippert, H.J., 1993. Vulkanismus im Devon des Rhenoherzynikums. Fazielle und paläogeographische Entwicklung vulkanisch geprägter mariner Becken am Beispiel des Lahn-Dill-Gebietes. In: Geologische Abhandlungen Hessen. 98. pp. 3–87.
Nieć, M., Pawlikowski, M., 2019. Dolomite-illitic rocks (dolillite) – the product of hydrothermal replacement of carbonate rocks in the Holy Cross Mts., Poland – a possible guide to ores. Geol. Q. 63, 275–295.
Over, D.J., Hopkins, T.H., Brill, A., Spaziani, A.L., 2003. Age of the Middlesex Shale (Upper Devonian, Frasnian) in New York State. Courier Forschungsinstitut Senckenberg 242, 217–223.
Paeckelmann, W., Kühne, F., 1936. Erläuterungen zu Blatt Madfeld. Geologische Karten von Preußen und benachbarten deutschen Ländern, 1:25 000. 4518 (79 pp.).
Pisarzowska, A., Racki, G., 2012. Isotopic geochemistry across the Early-Middle Frasnian transition (Late Devonian) on the South Polish carbonate shelf: a reference for the global punctata Event. Chem. Geol. 334, 199–220.
Pisarzowska, A., Sobstel, M., Racki, G., 2006. Conodont-based event stratigraphy of the Early-Middle Frasnian transition on the South Polish carbonate shelf. Acta Palaeontol. Pol. 51 (4), 609–646.
Pisarzowska, A., Berner, Z.A., Racki, G., 2014. Geochemistry of Early Frasnian (Late Devonian) pyrite-ammonoid level in the Kostomłoty Basin, Poland, and a new proxy parameter for assessing the relative amount of syngenetic and diagenetic pyrite. Sediment. Geol. 308, 18–31.
Polyansky, O.P., Prokopiev, A.V., Koroleva, O.V., Tomshin, M.D., Reverdatto, V.V., Selyatitsky, A.Y., Travin, A.V., Vasiliev, D.A., 2017. Temporal correlation between dyke swarms and crustal extension in the middle Palaeozoic Vilyui rift basin, Siberian platform. Lithos 282, 45–64.
Pyle, D.M., Mather, T.A., 2003. The importance of volcanic emissions for the global atmospheric mercury cycle. Atmos. Environ. 37, 5115–5124.
Racki, G., 2005. Toward understanding Late Devonian global events; few answers, many questions. In: Over, D.J., Morrow, J.R., Wignall, P.B. (Eds.), Understanding Late Devonian and Permian-Triassic Biotic and Climatic Events: Towards an Integrated Approach. Developments in Palaeontology and Stratigraphy 20. Elsevier, Amsterdam, pp. 5–36.
Racki, G., 2020. A volcanic scenario for the Frasnian–Famennian major biotic crisis and other Late Devonian global changes: more answers than questions? Global and Planetary Change 189, 103174.
Racki, G., Bultynck, P., 1993. Conodont biostratigraphy of the Middle to Upper Devonian boundary Beds in the Kielce area of the Holy Cross Mts. Acta Geol. Pol. 44, 1–25.
Racki, G., Piechota, A., Bond, D., Wignall, P., 2004. Geochemical and ecological aspects of lower Frasnian pyrite-ammonoid level at Kostomłoty (Holy Cross Mountains, Poland). Geol. Q. 48, 267–282.
Racki, G., Joachimski, M.M., Morrow, J.R., 2008. A major perturbation of the global carbon budget in the Early–Middle Frasnian transition (Late Devonian). Palaeogeogr. Palaeoclimatol. Palaeoecol. 269, 127–129.
Racki, G., Rakociński, M., Marynowski, L., Wignall, P.B., 2018. Mercury enrichments and the Frasnian-Famennian biotic crisis: a volcanic trigger proved? Geology 46, 543–546.
Rakociński, M., Pisarzowska, A., Janiszewska, K., Szrek, P., 2016. Depositional conditions during the Lower Kellwasser Event (Late Frasnian) in deep-shelf Łysogóry basin of the Holy Cross Mountains (Poland). Lethaia 49, 571–590.
Retallack, G.J., Huang, C., 2011. Ecology and evolution of Devonian trees in New York, USA. Palaeogeogr. Palaeoclimatol. Palaeoecol. 299, 110–128.
Ribbert, K.-H., Skupin, K., Oesterreich, B., 2006. Erläuterungen zu Blatt 4518 Madfeld, 2.,völlig neu bearbeitete Auflage. Geologische Karte von Nordrhein-Westfalen 1:25 000. 191 pp.. Krefeld (Geologischer Dienst NRW).
Sackett, W.M., Thompson, R.R., 1963. Isotope organic carbon composition of recent continental derived clastic sediments of Eastern Gulf Coast, Gulf of Mexico. Am. Assoc. Petrol. Geol. 147, 531–535.
Sageman, B.B., Murphy, A.E., Werne, J.P., Ver Straeten, C.A., Hollander, D.J., Lyons, T.W., 2003. A tale of shales: the relative roles of production, decomposition, and dilution in the accumulation of organic-rich strata, Middle–Upper Devonian, Appalachian basin. Chem. Geol. 195, 229–273.
Salamon, M., Königshof, P., 2010. Middle Devonian olistostromes in the Rheno-Hercynian zone (Rheinisches Schiefergebirge) – an indication of back arc rifting on the southern shelf of Laurussia. Gondwana Res. 14, 281–291.
Schobben, M., van de Schootbrugge, B., Wignall, P., 2019. Interpreting the Carbon Isotope Record of Mass Extinctions. Elements 15, 331–337.

Śliwiński, M.G., Whalen, M.T., Newberry, R.J., Payne, J.H., Day, J., 2011. Stable isotope ($\delta^{13}C_{carb\ \&\ org}$, $\delta^{15}N_{org}$) and trace element anomalies during the Late Devonian '*punctata* event' in the Western Canada Sedimentary Basin. Palaeogeogr. Palaeoclimatol. Palaeoecol. 307, 245–271.

Sim S., M., Ono, S., Hurtgen T., M., 2015. Sulfur isotope evidence for low and fluctuating sulfate levels intheLateDevonian ocean and the potential link with the mass extinctionevent. Earth and Planetary Science Letters 419, 52–62.

Śliwiński, M.G., Whalen, M.T., Meyer, F.J., Majs, F., 2012. Constraining clastic input controls on magnetic susceptibility and trace element anomalies during the Late Devonian punctata event in the Western Canada Sedimentary Basin. Terra Nova 24, 301–309.

Stritzke, R., 1989. Stratigraphie, Faziesanalyse und Paläogeographie im Oberdevon des Briloner Vorriffgebiets (Ostsauerland). In: Fortschritte in der Geologie von Rheinland und Westfalens. 35. pp. 75–106.

Stritzke, R., 1990. Die Karbonatsedimentation im Briloner Vorriffbereich. Geol. Jahrb. D95, 253–315.

Sunkel, G., 1990. Devonischer submariner Vulkanismus im Ostsauerland (Rheinisches Schiefergebirge): Vulkanaufbau, Magmenzusammensetzung und Alteration. Bochumer Geologische und Geotechnische Schriften. 34. pp. 1–250 11 pls.

Sweere, T., van den Sander, B., Dickson, A.J., Reichart, G.J., 2016. Definition of new trace-metal proxies for the controls on organic matter enrichment in marine sediments based on Mn, Co, Mo and Cd concentrations. Chem. Geol. 441, 235–245.

Szulczewski, M., 1971. Upper Devonian conodonts, stratigraphy and facial development in the Holy Cross Mts. Acta Geol. Pol. 21, 1–129.

Tomshin, M.D., Kopylova, A.G., Konstantinov, K.M., Gogoleva, S.S., 2018. Basites of the Vilyui paleorift: geochemistry and sequence of intrusive events. Russ. Geol. Geophys. 59, 1204–1216.

Tribovillard, N., Algeo, T.J., Baudin, F., Riboulleau, A., 2012. Analysis of marine environmental conditions based on molybdenum–uranium covariation. Applications to Mesozoic paleoceanography. Chem. Geol. 324–325, 46–58.

Tribovillard, N., Armynot du Châtelet, E., Gay, A., Barbecot, F., Sansjofre, P., Potdevin, J.-L., 2013. Geochemistry of cold seepage-impacted sediments: per-ascensum or per-descensum trace metal enrichment? Chem. Geol. 340, 1–12.

Vandelaer, E., Vandormael, C., Bultynck, P., 1989. Biofacies and Refinement of Conodont Succession in the Lower Frasnian (Upper Devonian) of the Type Area (Frasnes-Nismes, Belgium). Courier Forschungsinstitut Senckenberg 117, 321–351.

Vierek, A., 2007. Transitional reef-to-basin facies of Lower Frasnian limestones determined by microfacies analysis (Wietrznia, Holy Cross Mts, Poland). Facies 53, 141–155.

Vierek, A., Racki, G., 2011. Depositional versus ecological control on the conodont distribution in the Lower Frasnian forereef facies, Holy Cross Mountains, Poland. Palaeogeogr. Palaeoclimatol. Palaeoecol. 312, 1–23.

Von Raumer, J.F., Nesbor, H.-D., Stampfli, G.M., 2017. The north subducting Rheic Ocean during the Devonian: consequences for the Rhenohercynian ore sites. Int. J. Earth Sci. 106, 2279–2296.

Walliser, O.H., 1996. Global events in the Devonian and Carboniferous. In: Walliser, O.H. (Ed.), Global Events and Event Stratigraphy in the Phanerozoic. Springer, Berlin, pp. 225–250.

Wang, C.-Y., 1994. Application of the Frasnian standard Conodont Zonation in South China. Courier Forschungsinstitut Senckenberg 168, 83–129.

Warme, J.E., Sandberg, C.A., 1995. The catastrophic Alamo Breccia of Southern Nevada: record of a late Devonian extraterrestrial impact. Courier Forschungsinstitut Senckenberg 188, 31–57.

Wendt, J., Belka, Z., 1991. Age and Depositional Environment of Upper Devonian (Early Frasnian to Early Famennian) Black Shales and Limestones (Kellwasser Facies) in the Eastern Anti-Atlas, Morocco. – Facies. 25. pp. 51–90.

Wu, F.-Y., Arzamastsev, A.A., Mitchell, R.H., Li, Q.-L., Sun, J., Yang, Y.-H., Wang, R.-C., 2013. Emplacement age and Sr-Nd isotopic compositions of the Afrikanda alkaline ultramafic complex, Kola Peninsula, Russia. Chem. Geol. 353, 210–229.

Yans, J., Corfield, R.M., Racki, G., Préat, A., 2007. Evidence for a major perturbation of the carbon cycle in the Middle Frasnian *punctata* conodont Zone. Geol. Mag. 144, 263–270.

Zhuravlev, A.V., Sokiran, E.V., Evdokimova, I.O., Dorofeeva, L.A., Rusetskaya, G.A., Małkowski, K., 2006. Faunal and facies changes at the Early–Middle Frasnian boundary in the north – western east European Platform. Acta Palaeontol. Pol. 51 (4), 747–758.

Ziegler, W., 1958. Conodontenfeinstratigraphische Unter- suchungen an der Grenze Mitteldevon/Oberdevon und in der Adorf Stufe. NotizbI. hess. L.-A. Bodenforsch., Bd. 87.